Dynamic RF Chain Selection for Energy Efficient and Low Complexity Hybrid Beamforming in Millimeter Wave MIMO Systems

Aryan Kaushik, John Thompson, *Fellow, IEEE*, Evangelos Vlachos, *Member, IEEE*, Christos Tsinos, *Member, IEEE*, and Symeon Chatzinotas, *Senior Member, IEEE*

***Abstract*—This paper proposes a novel architecture with a framework that dynamically activates the optimal number of radio frequency (RF) chains used to implement hybrid beamforming in a millimeter wave (mmWave) multiple-input and multiple-output (MIMO) system. We use fractional programming to solve an energy efficiency maximization problem and exploit the Dinkelbach method (DM)-based framework to optimize the number of active RF chains and data streams. This solution is updated dynamically based on the current channel conditions, where the analog/digital (A/D) hybrid precoder and combiner matrices at the transmitter and the receiver, respectively, are designed using a codebook-based fast approximation solution called gradient pursuit (GP). The GP algorithm shows less run time and complexity while compared to the state-of-the-art orthogonal matching pursuit (OMP) solution. The energy and spectral efficiency performance of the proposed framework is compared with the existing state-of-the-art solutions, such as the brute force (BF), the digital beamformer, and the analog beamformer. The codebook-free approaches to design the precoders and combiners, such as alternating direction method of multipliers (ADMMs) and singular value decomposition (SVD)-based solution are also shown to be incorporated into the proposed framework to achieve better energy efficiency performance.**

***Index Terms*—RF chain selection, energy efficiency optimization, low complexity, hybrid precoding and combining, millimeter wave MIMO, 5G wireless.**

I. Introduction

THE EMERGING advanced consumer devices and developed communication systems have resulted in ever-increasing demands on bandwidth and capacity. For instance, Cisco's annual report suggests that mobile video traffic is expected to generate 74% of the global mobile data traffic by 2020 [1]. The microwave frequency spectrum at sub-6 GHz frequencies, which we currently make use of for mobile broadband, is limited to a very crowded frequency range enhancing the demand for an unused available spectrum which can be resolved by the use of millimeter wave (mmWave) frequency spectrum [2], [3]. The use of mmWave frequency bands appears to be a promising technology to meet the needs of fifth generation (5G) wireless communication systems such as increased capacity, high data rates, improved coverage, lower latency, high mobility, high reliability and lower infrastructure costs [4]–[6]. A few existing applications of the mmWave spectrum are in satellite communications, wireless backhaul, radio applications and radar communication. However, mmWave faces challenges of severe path loss, blocking effects, new hardware constraints and unconventional channel characteristics.

The high bandwidths for mmWave communication compared to sub-6 GHz frequency bands must be traded off against increased path loss [7], which can be compensated using large-scale antenna arrays [8], [9]. The large number of antenna elements and the high bandwidth makes it hard to use a separate radio frequency (RF) chain for each antenna due to the large requirements in power consumption and hardware complexity [8]. A conventional fully digital beamforming architecture used for sub-6 GHz frequencies requires a dedicated RF chain per antenna with the electronic components such as digital-to-analog converters (DACs) and analog-to-digital converters (ADCs) that enhances the hardware complexity and power consumption with the increase in antenna size [8], [9]. Thus, a digital beamforming architecture seems currently impractical to be implemented for large scale antenna arrays in the mmWave band.

As an alternative, an analog beamforming approach could be considered to solve this problem. The analog beamforming architecture involves a network of analog phase shifters with a single RF chain in the system [10], [11], which is highly advantageous to reduce hardware complexity and power consumption. But analog only beamforming approach cannot support multi-stream communication and the capacity performance is usually worse than the fully digital one. Furthermore, the support of multi-user communications is very difficult.

The performance of the mmWave multiple-input multiple-output (MIMO) systems can be significantly improved through

Manuscript received July 16, 2018; revised December 26, 2018, April 5, 2019, and July 23, 2019; accepted July 23, 2019. Date of publication July 29, 2019; date of current version November 20, 2019. This work was supported in part by the Engineering and Physical Sciences Research Council under Grant EP/P000703/1 and Grant EP/L026147/1, and in part by ECLECTIC project under FNR CORE Framework. The associate editor coordinating the review of this paper and approving it for publication was R. Vaze. *(Corresponding author: Aryan Kaushik.)*

A. Kaushik, J. Thompson, and E. Vlachos are with the Institute for Digital Communications, University of Edinburgh, Edinburgh EH9 3JL, U.K. (e-mail: a.kaushik@ed.ac.uk; j.s.thompson@ed.ac.uk; e.vlachos@ed.ac.uk).

C. Tsinos and S. Chatzinotas are with the Interdisciplinary Centre for Security, Reliability and Trust, University of Luxembourg, 1511 Luxembourg, Luxembourg (e-mail: christos.tsinos@uni.lu; symeon.chatzinotas@uni.lu).

Digital Object Identifier 10.1109/TGCN.2019.2931613

the use of analog/digital (A/D) hybrid beamforming architectures where the number of RF chains and associated ADCs/DACs are much less than the number of antennas [12], [13]. The A/D hybrid beamforming also enables spatial multiplexing and multi-user MIMO communication, and A/D hybrid transceiver solutions have recently been proposed to enable mmWave MIMO systems [14]–[16]. The A/D hybrid beamforming system can be implemented to provide satisfying rate performance by avoiding the discussed limitations of a fully digital solution [14]–[16]. One should note that we can reduce the power consumption by implementing low resolution quantization for both conventional and A/D hybrid beamforming architectures. To that end some approaches have been applied for energy efficiency maximization such as in [17]. Optimizing the number of RF chains further leverages the energy efficiency metric and reduces the gap between the spectral efficiency of A/D hybrid and fully digital beamforming architectures. Reference [18] suggests that the A/D hybrid beamforming architecture with low resolution DACs along with optimizing the number of RF chains shows better energy efficiency performance than the conventional digital beamforming architecture for 1-bit and 3-bits sampling resolutions.

To implement the A/D hybrid beamforming system which uses RF precoders based on the phase shifting networks, we can use the most popular structures such as the fully-connected and the partially-connected. The fully-connected structure connects all the antennas to each RF chain whereas the partially-connected structure connects only a subset of the antennas requiring less number of phase shifters [19]. The use of a partially-connected structure at the transceiver can further reduce the power consumption [16], for instance, our previous work [18] uses a partially-connected structure to evaluate the energy and rate performance where the partially-connected structure is opted to achieve high energy efficiency. This paper mainly uses the fully-connected structure to demonstrate the contributions of the proposed framework for a mmWave MIMO system. However, the energy efficiency performance using the partially-connected structure is also observed via simulations. We can observe from recent literature that there are works considering the energy efficient design of a A/D hybrid transceiver, however there is lack of works that optimize the number of RF chains which we discuss in the following subsection.

A. Literature Review

Reference [15] proposes a spectrally efficient A/D hybrid precoder design by maximizing the desired rate for fully-connected limited RF chain systems. However, it does not consider the energy consumption. For an energy efficient system, [20] considers a sub-connected architecture, where each RF chain is connected to only a subset of transmitter (TX) antennas requiring fewer phase shifters, but it does not discuss how to design an energy efficient precoder with a fully-connected architecture. Reference [19] considers both fully-connected and partially-connected structures to design a A/D hybrid precoder where the partially-connected structure seems to outperform fully-connected structure in terms of energy efficiency. However, it only considers the design of the precoder matrices and there is no emphasis on optimizing the number of RF chains which is a key factor for an energy efficient system.

The RF chains consume a large amount of power in wireless communication systems and increase the cost for these systems [21]. Reference [22] performs an energy efficient optimization to design a A/D hybrid precoder where to calculate the optimal number of RF chains, the full precoding solution is computed for all possible numbers of RF chains. This is referred to as the brute force (BF) technique throughout in this paper. References [15] and [22] use orthogonal matching pursuit (OMP) to optimize the precoder matrices. Alternative greedy strategies to OMP can be exploited to lower the complexity. A mmWave A/D hybrid MIMO system can be used for 5G mmWave MIMO applications such as cellular backhaul connections when we jointly optimize the number of RF chains and the A/D hybrid precoder and combiner matrices leading to a highly energy efficient system.

B. Contributions

This paper proposes an energy efficient A/D hybrid beamforming framework, where the RF precoder and baseband precoder matrices, and RF combiner and baseband combiner matrices are optimized along with the number of active RF chains but with low complexity. We use power allocation, and Dinkelbach method (DM) is implemented to optimize the number of RF chains. Fig. 1 shows the novel architecture with proposed framework for a mmWave single user fully-connected A/D hybrid beamforming MIMO system with digital baseband precoding and associated switches, followed by RF chains and associated DACs, and constrained RF precoding implemented using phase shifters network at the TX, and vice-versa at the receiver (RX). In this novel architecture, for a certain number of RF chains implemented in the hardware, the DM block drives digital switches to activate only those RF chains that we obtain as an optimal solution from the proposed method. In practice the digital switches would be a part of the digital processor. If the DM block is replaced by another method used to optimize the number of RF chains, the number of active RF chains and associated DACs/ADCs may be different.

To compute the A/D hybrid precoders and combiners, the proposed approach incorporates a codebook-based approach through one of the greedy strategies, i.e., gradient pursuit (GP) [23]. Simulations show that the proposed GP-based approach is a faster and less complex approach to compute the precoder and combiner matrices than the state of the art OMP. Furthermore, the proposed framework can also be incorporated with the existing codebook-free solutions such as alternating direction method of multipliers (ADMM) [16] and singular value decomposition (SVD) based solution [12]. The objective is to achieve better energy efficiency performance for codebook-free approaches over the fixed number of RF chains case. The proposed energy efficient and low complexity A/D

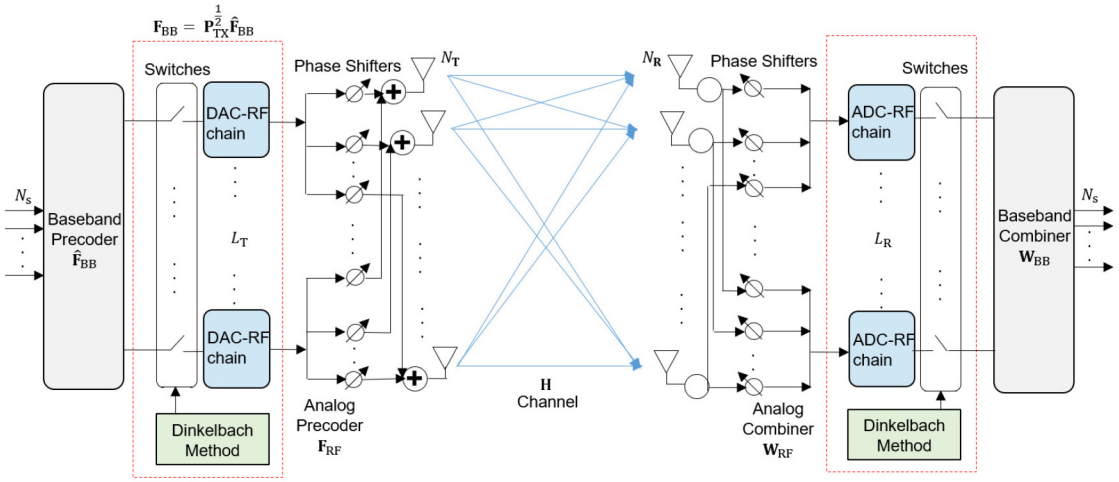

(a) The fully-connected A/D hybrid beamforming architecture with the proposed framework.

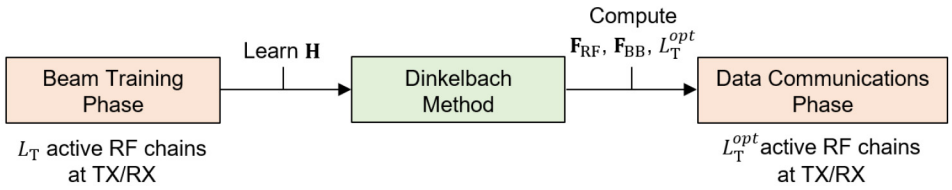

(b) Block diagram of the beam tracking phase and the data communications phase.

Fig. 1. System model for a mmWave A/D hybrid MIMO system with the proposed framework.

hybrid precoder framework with a fully-connected architecture can be used in designing 5G mmWave MIMO systems effectively and efficiently, such as in 5G cellular systems and wireless backhaul networks.

The main contributions of this paper can be summarized as follows:

1) The paper proposes a novel algorithmic framework, where the number of active RF chains is dynamically adapted on a frame-by-frame basis. This is carried out using a low complexity alternative to brute force optimization [22] based on the current channel conditions measured in the A/D hybrid beamforming architecture.
2) We develop a reduced complexity DM based solution to find the optimal number of RF chains and streams for the mmWave MIMO system for the current channel conditions.
3) A GP-based approach is proposed as a lower complexity approximation solution to compute the precoder and combiner matrices than the state of the art OMP solution.

Outline: Section II describes the channel and system model implemented for the novel architecture. Section III discusses the low complexity design of the A/D hybrid precoder and combiner matrices using GP algorithm. Section IV provides the energy efficiency maximization problem and we solve the optimization problem via the DM based solution used in the framework where Section IV-A discusses the energy efficiency computation, while Section IV-B describes the energy efficient and low complexity solution to optimize the number of RF chains and activate that many RF chains in the system (as shown in Fig. 1). Section V provides the simulation results. The conclusions are provided in Section VI.

Notations: $\mathbf{A}$, $\mathbf{a}$ and a stand for a matrix, a vector and a scalar, respectively; $\mathbf{A}^{(i)}$ represents the i^{th} column of $\mathbf{A}$; transpose, complex conjugate transpose and pseudo inverse of $\mathbf{A}$ are denoted as $\mathbf{A}^T$, $\mathbf{A}^H$ and $\mathbf{A}^\dagger$, respectively; $\|\mathbf{A}\|_F$, tr($\mathbf{A}$) and $|\mathbf{A}|$ represent the Frobenius norm, trace, and determinant of $\mathbf{A}$, respectively; $\|\mathbf{a}\|_p$ is the p-norm of $\mathbf{a}$; $[\mathbf{A}|\mathbf{B}]$ denotes horizontal concatenation; $x \cup y$ denotes the union of x and y union disjoint sets; $\mathbf{A}|_\Gamma$ denotes a matrix consisting of rows of matrix $\mathbf{A}$ with indices from Γ set; diag($\mathbf{A}$) generates a vector by the diagonal elements of $\mathbf{A}$; $\mathbf{I}_N$ and $\mathbf{0}_{X\times Y}$ represent $N \times N$ identity matrix and $X \times Y$ all-zeros matrix, respectively; $\mathcal{CN}(\mathbf{a}; \mathbf{A})$ denotes a vector of complex Gaussian random variables with mean $\mathbf{a}$ and covariance matrix $\mathbf{A}$, and i.i.d. shows that the entries of a vector of random variables are independent and identically distributed. $\mathbf{X} \in \mathbb{C}^{A\times B}$ and $\mathbf{X} \in \mathbb{R}^{A\times B}$ denote $A \times$ B size $\mathbf{X}$ matrix with complex and real entries, respectively; the expectation operator and the real part of a complex variable are denoted as $\mathbb{E}\{\cdot\}$ and $\mathbb{R}\{\cdot\}$, respectively.

II. MmWave A/D Hybrid MIMO Model

A. MmWave Channel Model

Let us consider a single user MIMO system with N_{T} antennas at the TX, sending N_{s} data streams to a system with N_{R} RX antennas. The fading channel models used in traditional MIMO becomes inaccurate for mmWave channel modeling

due to the high free-space path loss and large tightly-packed antenna arrays. The existing literature mostly addresses the narrowband clustered channel model [24], [25] for mmWave propagation due to different channel settings such as number of multipaths, amplitudes, etc. such as in [8], [15].

For N_{cl} clusters and N_{ray} propagation paths in each cluster and for a uniform linear array (ULA) antenna elements, the mmWave channel matrix is defined as follows:

$$\mathbf{H} = \sqrt{\frac{N_{\mathrm{T}}N_{\mathrm{R}}}{N_{\mathrm{cl}}N_{\mathrm{ray}}}} \sum_{i=1}^{N_{\mathrm{cl}}} \sum_{l=1}^{N_{\mathrm{ray}}} \alpha_{il} \mathbf{a}_{\mathrm{R}}(\phi_{il}^{r}) \mathbf{a}_{\mathrm{T}}\left(\phi_{il}^{t}\right)^{H}, \tag{1}$$

where α_{il} denotes the gain of *l*-th ray in *i*-th cluster and it is assumed that α_{il} are i.i.d. $\mathcal{CN}(0, \sigma_{\alpha,i}^2)$, where $\sigma_{\alpha,i}^2$ is average power of the *i*-th cluster such that $\sum_{i=1}^{N_{\mathrm{cl}}} \sigma_{\alpha,i}^2 = \gamma$, where $\gamma = \sqrt{\frac{N_{\mathrm{T}}N_{\mathrm{R}}}{N_{\mathrm{cl}}N_{\mathrm{ray}}}}$, is the normalization factor satisfying $\mathbb{E}\{\|\mathbf{H}\|_F^2\} = 1/\sqrt{N_{\mathrm{cl}}N_{\mathrm{ray}}}$. Further, $\mathbf{a}_{\mathrm{R}}(\phi_{il}^{r})$ and $\mathbf{a}_{\mathrm{T}}(\phi_{il}^{t})$ represent the normalized receive and transmit array response vectors, where ϕ_{il}^{t} and ϕ_{il}^{r} are the azimuth angles of departure and arrival, respectively. The antenna elements at the TX and the RX can be modeled as ideal sectored elements [26] and then antenna element gains can be evaluated over ideal sectors. In (1), the transmit and receive antenna element gains are considered unity over ideal sectors defined by $\phi_{il}^{t} \in [\phi_{\min}^{t}, \phi_{\max}^{t}]$ and $\phi_{il}^{r} \in [\phi_{\min}^{r}, \phi_{\max}^{r}]$, respectively. For a N_{Z}-element ULA on *Z*-axis, the array response vector can be expressed as [27]: $\mathbf{a}_{\mathrm{Z}}(\phi) = \frac{1}{\sqrt{N_{\mathrm{Z}}}} e^{jm\frac{2\pi}{\lambda}d\sin(\phi)^{T}}$, where $0 \leq m \leq (N_{\mathrm{Z}}-1)$ is a real integer, d is the inter-element spacing in wavelengths and λ is the signal wavelength. The array response vectors can also be computed using other array geometries such as rectangular array and circular array. As mentioned above, we assume perfect channel knowledge at the TX and the RX [15], [16], [22]. However, this work can also be extended to consider channel estimation errors, for example, [28] proposes an efficient channel estimation algorithm for hybrid architecture mmWave systems.

The beamspace representation [29], [30] of the narrowband channel can be written as follows:

$$\mathbf{H} = \mathbf{D}_{\mathrm{R}}\mathbf{H}_{\mathrm{v}}\mathbf{D}_{\mathrm{T}}^{H}, \tag{2}$$

where $\mathbf{H}_{\mathrm{v}} \in \mathbb{C}^{L_{\mathrm{R}} \times L_{\mathrm{T}}}$ represents a sparse matrix with a few non-zero entries, while $\mathbf{D}_{\mathrm{R}} \in \mathbb{C}^{N_{\mathrm{R}} \times L_{\mathrm{R}}}$ and $\mathbf{D}_{\mathrm{T}} \in \mathbb{C}^{N_{\mathrm{T}} \times L_{\mathrm{T}}}$ are the discrete Fourier transform (DFT) matrices.

B. A/D Hybrid MIMO System Model

In large-scale MIMO communication systems, based on the A/D hybrid precoding scheme, the number of RF chains is larger than or equal to the number of baseband data streams and smaller than or equal to the number of TX antennas. L_{T} denotes the number of available RF chains at the TX with the limitation that $N_{\mathrm{s}} \leq L_{\mathrm{T}} \leq N_{\mathrm{T}}$ and similarly L_{R} is for the RX with the condition $N_{\mathrm{s}} \leq L_{\mathrm{R}} \leq N_{\mathrm{R}}$. We consider the number of RF chains at the RX to be same as at the TX, i.e., $L_{\mathrm{R}} = L_{\mathrm{T}}$.

Let $\mathbf{F}_{\mathrm{BB}} = \mathbf{P}_{\mathrm{TX}}^{\frac{1}{2}}\hat{\mathbf{F}}_{\mathrm{BB}}$ denote the baseband precoder matrix which inputs to the DAC-RF chain block where $\mathbf{P}_{\mathrm{TX}} \in \mathbb{R}^{L_{\mathrm{T}} \times L_{\mathrm{T}}}$ is a diagonal matrix of power allocation values with $\mathrm{tr}(\mathbf{P}_{\mathrm{TX}}) = P_{\max}$, $\hat{\mathbf{F}}_{\mathrm{BB}}$ is the digital precoding matrix before the switches, and $\mathbf{F}_{\mathrm{RF}}$ denotes the RF precoder matrix. $\mathbf{F}_{\mathrm{BB}}$ has dimensions of $L_{\mathrm{T}} \times N_{\mathrm{s}}$ using its L_{T} transmit chains and $\mathbf{F}_{\mathrm{RF}}$ has dimensions of $N_{\mathrm{T}} \times L_{\mathrm{T}}$ using the phase shifting network. Similarly at the RX, the matrices $\mathbf{W}_{\mathrm{BB}}$ and $\mathbf{W}_{\mathrm{RF}}$ denote the $L_{\mathrm{R}} \times N_{\mathrm{s}}$ baseband combiner and the $N_{\mathrm{R}} \times L_{\mathrm{R}}$ RF combiner, respectively. The TX symbol vector $\mathbf{s} \in \mathbb{C}^{N_{\mathrm{s}} \times 1}$ is such that $\mathbb{E}\{\mathbf{s}\mathbf{s}^{H}\} = \frac{1}{N_{\mathrm{s}}}\mathbf{I}_{N_{\mathrm{s}}}$. All elements of $\mathbf{F}_{\mathrm{RF}}$ and $\mathbf{W}_{\mathrm{RF}}$ are of constant modulus. The power constraint at the TX is satisfied by $\|\mathbf{F}_{\mathrm{RF}}\mathbf{F}_{\mathrm{BB}}\|_F^2 = P_{\max}$, where $P_{\max}$ is the maximum allocated power. We assume a unit magnitude and continuous phase constraint on the phase shifters [15].

Consider a narrowband propagation channel with $\mathbf{H}$ as the $N_{\mathrm{R}} \times N_{\mathrm{T}}$ channel matrix, which is assumed to be known to both the TX and the RX, then the received signal can be expressed as follows:

$$\mathbf{y} = \mathbf{H}\mathbf{F}_{\mathrm{RF}}\mathbf{F}_{\mathrm{BB}}\mathbf{s} + \mathbf{n}, \tag{3}$$

where $\mathbf{y}$ is the $N_{\mathrm{R}} \times 1$ received vector and $\mathbf{n}$ is a $N_{\mathrm{R}} \times 1$ noise vector with entries which are modeled as i.i.d. $\mathcal{CN}(0, \sigma_{\mathrm{n}}^2)$. After the application of the combining matrices, the received signal can be written as follows:

$$\tilde{\mathbf{y}} = \mathbf{W}_{\mathrm{BB}}^{H}\mathbf{W}_{\mathrm{RF}}^{H}\mathbf{y} = \mathbf{W}_{\mathrm{BB}}^{H}\mathbf{W}_{\mathrm{RF}}^{H}\mathbf{H}\mathbf{F}_{\mathrm{RF}}\mathbf{F}_{\mathrm{BB}}\mathbf{s} + \mathbf{W}_{\mathrm{BB}}^{H}\mathbf{W}_{\mathrm{RF}}^{H}\mathbf{n}. \tag{4}$$

In the following section, we discuss the low complexity designs of A/D hybrid precoders, i.e., $\mathbf{F}_{\mathrm{RF}}, \mathbf{F}_{\mathrm{BB}}$, and A/D hybrid combiners, i.e., $\mathbf{W}_{\mathrm{RF}}, \mathbf{W}_{\mathrm{BB}}$.

III. Low Complexity A/D Hybrid Precoders and Combiners Design

The combined problem of designing the precoders and combiners and the number of RF chains can be partitioned into three sub-problems:

- to optimize the A/D hybrid precoders $\mathbf{F}_{\mathrm{RF}}\mathbf{F}_{\mathrm{BB}}$,
- to optimize the A/D hybrid combiners $\mathbf{W}_{\mathrm{RF}}\mathbf{W}_{\mathrm{BB}}$ and
- to optimize the number of RF chains, i.e., obtaining L_{T}^{opt} at the TX and L_{R}^{opt} at the RX.

Firstly in this section, we focus on designing the A/D hybrid precoder matrices $\mathbf{F}_{\mathrm{RF}}$ and $\mathbf{F}_{\mathrm{BB}}$ as shown in Section III-A and the hybrid combiner matrices $\mathbf{W}_{\mathrm{RF}}$ and $\mathbf{W}_{\mathrm{BB}}$ as shown in Section III-B by assuming that L_{T}^{opt} and L_{R}^{opt} are computed from the proposed DM based solution in Section IV already. In the next section, we propose the DM based solution for optimizing the number of RF chains at the TX and consider that $L_{\mathrm{R}}^{opt} = L_{\mathrm{T}}^{opt}$.

A. A/D Hybrid Precoding at the TX

It is known that the precoding matrix for the digital beamformer is given based on the singular value decomposition (SVD) of the channel matrix. We consider channel's SVD as $\mathbf{H} = \mathbf{U}_{\mathrm{H}}\mathbf{\Sigma}_{\mathrm{H}}\mathbf{V}_{\mathrm{H}}^{H}$, where $\mathbf{U}_{\mathrm{H}} \in \mathbb{C}^{N_{\mathrm{R}} \times N_{\mathrm{R}}}$ and $\mathbf{V}_{\mathrm{H}} \in \mathbb{C}^{N_{\mathrm{T}} \times N_{\mathrm{T}}}$ are unitary matrices, and $\mathbf{\Sigma}_{\mathrm{H}} \in \mathbb{R}^{N_{\mathrm{R}} \times N_{\mathrm{T}}}$ is a rectangular matrix of singular values in decreasing order whose diagonal elements are non-negative real numbers and whose non-diagonal elements are zero. The optimal fully digital precoding

matrix $\mathbf{F}_{\rm opt} = \mathbf{V}_{\rm H1}\mathbf{P}_{\rm TX}^{(1/2)}$ where the matrix $\mathbf{V}_{\rm H1} \in \mathbb{C}^{N_{\rm T}\times N_{\rm s}}$ consists of the $N_{\rm s}$ columns of the right singular matrix $\mathbf{V}_{\rm H}$ [15] and $\mathbf{P}_{\rm TX}$ is a diagonal matrix where each diagonal entry represents the power of each transmission stream for the digital precoding case with $\left\|\mathbf{F}_{\rm opt}\right\|_F^2 = {\rm tr}(\mathbf{P}_{\rm TX}) = P_{\max}$. We discuss about $\mathbf{P}_{\rm TX}$ in more details in the next section. In this section we assume that $\mathbf{P}_{\rm TX}$ is known.

In order to design the near-optimal A/D hybrid precoder, it can be assumed that the decomposition $\mathbf{F}_{\rm RF}\mathbf{F}_{\rm BB}$ can be made sufficiently close to the optimal fully digital precoding matrix $\mathbf{F}_{\rm opt}$ [15]. The Euclidean distance problem is a good approximation, so we can consider the Euclidean distance between the A/D hybrid precoder $\mathbf{F}_{\rm RF}\mathbf{F}_{\rm BB}$ and the channel's optimal fully digital precoder $\mathbf{F}_{\rm opt}$ to optimize the A/D hybrid precoder matrices. We can define $\mathcal{F}_{\rm RF}$ to be a set of basis vectors $\mathbf{a}_{\rm T}(\tilde{\phi}_{il}^t)$ in order to find the best low dimensional representation of the optimal matrix $\mathbf{F}_{\rm opt}$ where $\tilde{\phi}_{il}^t$ are the angles from the DFT codebook. The problem to design the A/D hybrid precoders can be stated as follows [14], [15]:

$$\begin{aligned}\left(\mathbf{F}_{\rm RF}^{opt}, \mathbf{F}_{\rm BB}^{opt}\right) = \underset{\mathbf{F}_{\rm RF},\mathbf{F}_{\rm BB}}{\rm argmin}\ & \left\|\mathbf{F}_{\rm opt} - \mathbf{F}_{\rm RF}\mathbf{F}_{\rm BB}\right\|_F^2, \\ {\rm s.t.}\ & \mathbf{F}_{\rm RF} \in \mathcal{F}_{\rm RF}, \|\mathbf{F}_{\rm RF}\mathbf{F}_{\rm BB}\|_F^2 \\ & = P_{\max}. \end{aligned} \tag{5}$$

We consider two stages in the system model as shown in Fig. 1: a) the beam training phase, and b) the data communications phase. In stage a), firstly $L_{\rm T}$ available RF chains are activated and the channel is computed which provides us the optimal beamformer, i.e., $\mathbf{F}_{\rm opt}$. Then the SVD of the channel is computed and the proposed DM is performed to obtain $L_{\rm T}^{opt}$. In stage b), the optimal analog and digital precoder matrices $\mathbf{F}_{\rm RF}^{opt}$ and $\mathbf{F}_{\rm BB}^{opt}$, respectively, are obtained using $L_{\rm T}^{opt}$. Note that, if we assume that the TX is active for stage a) a small proportion of time, for example, <10%, then the overall transmit energy consumption is dominated by stage b). The previous problem can be cast in the following form, given by:

$$\begin{aligned}\tilde{\mathbf{F}}_{\rm BB}^{opt} = \underset{\tilde{\mathbf{F}}_{\rm BB}}{\rm argmin}\ & \left\|\mathbf{F}_{\rm opt} - \tilde{\mathbf{D}}_{\rm T}\tilde{\mathbf{F}}_{\rm BB}\right\|_F^2, \\ {\rm s.t.}\ & \left\|{\rm diag}\left(\tilde{\mathbf{F}}_{\rm BB}\tilde{\mathbf{F}}_{\rm BB}^H\right)\right\|_0 = L_{\rm T}^{opt}, \left\|\tilde{\mathbf{D}}_{\rm T}\tilde{\mathbf{F}}_{\rm BB}\right\|_F^2 \\ & = P_{\max}, \end{aligned} \tag{6}$$

where $\tilde{\mathbf{D}}_{\rm T} \in \mathbb{C}^{N_{\rm T}\times L_{\rm T}^{opt}}$ is the matrix composed by the $L_{\rm T}^{opt}$ columns of the DFT matrix $\mathbf{D}_{\rm T}$ and $\tilde{\mathbf{F}}_{\rm BB}$ is a $L_{\rm T}^{opt} \times N_{\rm s}$ matrix. The matrices $\tilde{\mathbf{D}}_{\rm T}$ and $\tilde{\mathbf{F}}_{\rm BB}$ act as auxiliary variables from which we obtain $\mathbf{F}_{\rm RF}^{opt}$ and $\mathbf{F}_{\rm BB}^{opt}$, respectively. The sparsity constraint $\left\|{\rm diag}(\tilde{\mathbf{F}}_{\rm BB}\tilde{\mathbf{F}}_{\rm BB}^H)\right\|_0 = L_{\rm T}^{opt}$ suggests that $\tilde{\mathbf{F}}_{\rm BB}$ can not have more than $L_{\rm T}^{opt}$ non-zero rows. Thus, only $L_{\rm T}^{opt}$ columns of the DFT matrix $\mathbf{D}_{\rm T}$ are effectively selected which is given by $\tilde{\mathbf{D}}_{\rm T}$. Therefore, $L_{\rm T}^{opt}$ non-zero rows of $\tilde{\mathbf{F}}_{\rm BB}$ will give us the baseband precoder matrix $\mathbf{F}_{\rm BB}^{opt}$ and the columns of $\tilde{\mathbf{D}}_{\rm T}$ will provide the RF precoder matrix $\mathbf{F}_{\rm RF}^{opt}$. The optimal number of RF chains, i.e., $L_{\rm T}^{opt}$, is obtained from the proposed optimization solution derived in Section IV.

As shown in [15], (6) basically reformulates (5) into a sparsity constrained reconstruction problem with one variable. The problem can be now addressed as a sparse approximation problem [31] and OMP [32] can be used as an algorithmic solution. To develop fast approximate OMP algorithms that are less complex, [23] proposes improvements to greedy strategies using directional pursuit methods and discusses optimization schemes on basis of gradient, conjugate gradient and approximate conjugate gradient approaches. GP approach is implemented as an alternative solution to the optimization objective exhibiting similar performance as OMP, faster processing time and lower complexity. GP avoids matrix inversion by using only one matrix vector multiplication per iteration.

Algorithm 1 A/D Hybrid Precoder Design Through Gradient Pursuit (GP)

1: **Input:** $\mathbf{F}_{\rm opt}$, $\tilde{\mathbf{D}}_{\rm T}$, $L_{\rm T}^{opt}$
2: $\mathbf{F}_{\rm RF} = \mathbf{0}_{N_{\rm T}\times L_{\rm T}^{opt}}$, $\Gamma = \varnothing$
3: $\mathbf{F}_{\rm res} = \mathbf{F}_{\rm opt}$, $\mathbf{F}_{\rm BB} = \mathbf{0}_{L_{\rm T}^{opt}\times N_{\rm s}}$
4: **for** $i \le L_{\rm T}^{opt}$
5: $\quad\boldsymbol{\Psi} = \tilde{\mathbf{D}}_{\rm T}^H\mathbf{F}_{\rm res}$
6: $\quad k = {\rm argmax}_{l=1,\ldots,L_{\rm T}^{opt}}(\boldsymbol{\Psi}\boldsymbol{\Psi}^H)_{l,l}$
7: $\quad\mathbf{F}_{\rm RF} = [\mathbf{F}_{\rm RF} \mid \tilde{\mathbf{D}}_{\rm T}^{(k)}]$
8: $\quad\mathbf{D} = \mathbf{F}_{\rm RF}^H\mathbf{F}_{\rm res}$
9: $\quad\mathbf{C} = \mathbf{F}_{\rm RF}\mathbf{D}$
10: $\quad g = \frac{{\rm tr}\{\mathbf{F}_{\rm res}^H\mathbf{C}\}}{\|\mathbf{C}\|_F^2}$
11: $\quad\Gamma = \Gamma \cup k$
12: $\quad\mathbf{F}_{\rm BB}|_\Gamma = \mathbf{F}_{\rm BB}|_\Gamma - g\mathbf{D}$
13: $\quad\mathbf{F}_{\rm res} = \mathbf{F}_{\rm res} - g\mathbf{C}$
14: **end for**
15: $\mathbf{F}_{\rm BB} = \sqrt{P_{\max}}\frac{\mathbf{F}_{\rm BB}}{\|\mathbf{F}_{\rm RF}\mathbf{F}_{\rm BB}\|_F^2}$

Algorithm 1 starts by finding the k-th column of $\tilde{\mathbf{D}}_{\rm T}$, denoted as $\tilde{\mathbf{D}}_{\rm T}^{(k)}$, along which the optimal precoder has the maximum projection and then concatenates that selected column vector to the RF precoder $\mathbf{F}_{\rm RF}$ as shown in Step 6. The gradient direction in Step 7 is computed at each iteration and the step-size is determined explicitly making use of the gradient direction, as shown in Step 9. The index set Γ is updated at each iteration as shown in Step 10 which is used to generate the baseband precoder matrix $\mathbf{F}_{\rm BB}$. The residual precoding matrix is computed at Step 12 and the algorithm continues until all $L_{\rm T}^{opt}$ RF chains have been used. Finally the RF precoder matrix $\mathbf{F}_{\rm RF}$ and the baseband precoder matrix $\mathbf{F}_{\rm BB}$ are obtained at the end of the algorithm. The transmit power constraint is satisfied at Step 14.

B. A/D Hybrid Combining at the RX

The A/D hybrid combiner design has a similar mathematical formulation except that the transmit power constraint no longer applies. One may note here that by assuming the A/D hybrid precoders $\mathbf{F}_{\rm RF}\mathbf{F}_{\rm BB}$ to be fixed, the A/D hybrid combiners $\mathbf{W}_{\rm RF}\mathbf{W}_{\rm BB}$ can be designed in order to minimize the mean-squared-error (MSE) between the transmitted and processed received signals by using the linear minimum mean-square error (MMSE) RX [14], [15]. The optimization of the number of RF chains at the RX can be performed similarly as at

Algorithm 2 A/D Hybrid Combiner Design Through Gradient Pursuit (GP)

1: **Input:** $\mathbf{W}_{\mathrm{mmse}}$, $\tilde{\mathbf{D}}_{\mathrm{R}}$, L_{R}^{opt}
2: $\mathbf{W}_{\mathrm{RF}} = \mathbf{0}_{N_{\mathrm{R}} \times L_{\mathrm{R}}^{opt}}$, $\Gamma = \varnothing$
3: $\mathbf{W}_{\mathrm{res}} = \mathbf{W}_{\mathrm{mmse}}$, $\mathbf{W}_{\mathrm{BB}} = \mathbf{0}_{L_{\mathrm{R}}^{opt} \times N_{\mathrm{s}}}$
4: **for** $i \leq L_{\mathrm{R}}^{opt}$
5: $\quad \mathbf{\Psi} = \tilde{\mathbf{D}}_{\mathrm{R}}^{H} \mathbb{E}[\mathbf{y}\mathbf{y}^{H}] \mathbf{W}_{\mathrm{res}}$
6: $\quad k = \mathrm{argmax}_{l=1,\ldots,L_{\mathrm{R}}^{opt}} (\mathbf{\Psi}\mathbf{\Psi}^{H})_{l,l}$
7: $\quad \mathbf{W}_{\mathrm{RF}} = [\mathbf{W}_{\mathrm{RF}} \mid \tilde{\mathbf{D}}_{\mathrm{R}}^{(k)}]$
8: $\quad \mathbf{D} = \mathbf{W}_{\mathrm{RF}}^{H} \mathbf{W}_{\mathrm{res}}$
9: $\quad \mathbf{C} = \mathbf{W}_{\mathrm{RF}} \mathbf{D}$
10: $\quad g = \frac{\mathrm{tr}\{\mathbf{W}_{\mathrm{res}}^{H} \mathbf{C}\}}{\|\mathbf{C}\|_{F}^{2}}$
11: $\quad \Gamma = \Gamma \cup k$
12: $\quad \mathbf{W}_{\mathrm{BB}}|_{\Gamma} = \mathbf{W}_{\mathrm{BB}}|_{\Gamma} - g\mathbf{D}$
13: $\quad \mathbf{W}_{\mathrm{res}} = \mathbf{W}_{\mathrm{res}} - g\mathbf{C}$
14: **end for**

the TX. The design problem for combining matrices can be written as follows:

$$\left(\mathbf{W}_{\mathrm{RF}}^{opt}, \mathbf{W}_{\mathrm{BB}}^{opt}\right) = \underset{\mathbf{W}_{\mathrm{RF}}, \mathbf{W}_{\mathrm{BB}}}{\mathrm{argmin}} \ \mathbb{E}\left[\left\|\mathbf{s} - \mathbf{W}_{\mathrm{BB}}^{H} \mathbf{W}_{\mathrm{RF}}^{H} \mathbf{y}\right\|_{2}^{2}\right], \quad \text{s.t.} \ \ \mathbf{W}_{\mathrm{RF}} \in \mathcal{W}_{\mathrm{RF}}, \tag{7}$$

where $\mathcal{W}_{\mathrm{RF}}$ is defined similarly to $\mathcal{F}_{\mathrm{RF}}$ for TX. Following the steps in [15] and similar to the precoder optimization, the MMSE estimation problem may be further written as follows:

$$\tilde{\mathbf{W}}_{\mathrm{BB}}^{opt} = \underset{\tilde{\mathbf{W}}_{\mathrm{BB}}}{\mathrm{argmin}} \left\|\mathbb{E}\left[\mathbf{y}\mathbf{y}^{H}\right]^{\frac{1}{2}} \mathbf{W}_{\mathrm{mmse}} - \mathbb{E}\left[\mathbf{y}\mathbf{y}^{H}\right]^{\frac{1}{2}} \tilde{\mathbf{D}}_{\mathrm{R}} \tilde{\mathbf{W}}_{\mathrm{BB}}\right\|_{F}^{2} \quad \text{s.t.} \ \ \left\|\mathrm{diag}\left(\tilde{\mathbf{W}}_{\mathrm{BB}} \tilde{\mathbf{W}}_{\mathrm{BB}}^{H}\right)\right\|_{0} = L_{\mathrm{R}}^{opt}, \tag{8}$$

where $\tilde{\mathbf{D}}_{\mathrm{R}}$ is the DFT matrix and $\tilde{\mathbf{W}}_{\mathrm{BB}}$ is a $L_{\mathrm{R}}^{opt} \times N_{\mathrm{s}}$ matrix. The exact solution to (8) yields $\mathbf{W}_{\mathrm{mmse}}^{H}$ as follows [15]:

$$\mathbf{W}_{\mathrm{mmse}}^{H} = \left(\mathbf{F}_{\mathrm{BB}}^{H} \mathbf{F}_{\mathrm{RF}}^{H} \mathbf{H}\mathbf{H}^{H} \mathbf{F}_{\mathrm{RF}} \mathbf{F}_{\mathrm{BB}} + \sigma_{\mathrm{n}}^{2} N_{\mathrm{s}} \mathbf{I}_{N_{\mathrm{s}}}\right)^{-1} \times \mathbf{F}_{\mathrm{BB}}^{H} \mathbf{F}_{\mathrm{RF}}^{H} \mathbf{H}^{H}. \tag{9}$$

Similar to the sparsity reconstruction problem for the TX, L_{R}^{opt} non-zero rows of $\tilde{\mathbf{W}}_{\mathrm{BB}}$ will give us the baseband combiner matrix $\mathbf{W}_{\mathrm{BB}}^{opt}$ and the corresponding L_{R}^{opt} columns of $\mathbf{D}_{\mathrm{R}}$ will provide the RF combiner matrix $\mathbf{W}_{\mathrm{RF}}^{opt}$. This sparse signal recovery problem can again be solved by the GP algorithm.

Algorithm 2 provides the pseudo code of the GP solution to find the combiner matrices. It should be noted that step 14 of Algorithm 1 does not need to be replicated here as there is no power constraint at the RX unlike at the TX. It starts by finding the k-th column of $\tilde{\mathbf{D}}_{\mathrm{R}}$, denoted as $\tilde{\mathbf{D}}_{\mathrm{R}}^{(k)}$, along which the optimal combiner has the maximum projection which requires the received signal as well for computation, and then concatenates that selected column vector to the RF combiner $\mathbf{W}_{\mathrm{RF}}$ as shown in Step 6. The gradient direction in Step 7 is computed at each iteration and the step-size is determined explicitly making use of the gradient direction as shown in Step 9. Similar to the TX case, the index set Γ is updated at each iteration in Step 10 which is used to generate baseband combiner matrix $\mathbf{W}_{\mathrm{BB}}$. The residual precoding matrix is computed at Step 12. Finally the RF combiner matrix $\mathbf{W}_{\mathrm{RF}}$ and the baseband combiner matrix $\mathbf{W}_{\mathrm{BB}}$ are obtained at the end of the algorithm. In the next section we discuss on obtaining the optimal number of RF chains.

IV. Maximization of the Energy Efficiency via Dynamic Power Allocation

In this section we derive the proposed approach which aims at the maximization of the energy efficiency (EE) by dynamic power allocation in the baseband domain. In terms of achievable information rate *R* and consumed power *P*, the EE for the A/D hybrid design can be computed as follows:

$$\mathrm{EE}(\mathbf{P}_{\mathrm{TX}}) \triangleq \frac{R(\mathbf{P}_{\mathrm{TX}})}{P(\mathbf{P}_{\mathrm{TX}})} (\mathrm{bits/Hz/J}), \tag{10}$$

where *R* represents the information rate in bits/s/Hz and *P* is the required power in Watts (W).

The proposed design, as depicted in Fig. 1, describes a A/D hybrid system for the TX and the RX, with a certain number of RF chains L_{T} implemented in the hardware. The selection mechanism between the available RF chains is implemented in the baseband domain, as part of the digital processor. This procedure is driven by the DM block, which describes the optimal power scheme for each channel realization.

The power allocation at the TX can be described mathematically by using a diagonal sparse matrix $\mathbf{P}_{\mathrm{TX}} \in \mathcal{D}^{L_{\mathrm{T}} \times L_{\mathrm{T}}}$ where $\mathcal{D}^{L_{\mathrm{T}} \times L_{\mathrm{T}}} \subset \mathbb{R}^{L_{\mathrm{T}} \times L_{\mathrm{T}}}$ denotes the set of $L_{\mathrm{T}} \times L_{\mathrm{T}}$ diagonal sparse matrices. To represent the baseband selection mechanism we consider that $[\mathbf{P}_{\mathrm{TX}}]_{kk} \in [0, P_{\max}]$, for $k = 1, \ldots, L_{\mathrm{T}}$, where $P_{\max} = \mathrm{tr}(\mathbf{P}_{\mathrm{TX}})$. The diagonal entries of $\mathbf{P}_{\mathrm{TX}}$ with a zero value represent an open switch in Fig. 1. Thus, the non-zero diagonal values of $\mathbf{P}_{\mathrm{TX}}$ determine the number of the active RF chains for the TX, i.e., $L_{\mathrm{T}}^{opt} = \|\mathbf{P}_{\mathrm{TX}}\|_{0}$. If we increase the number of RF chains we might achieve a higher information rate but there is also higher power consumption. Hence, maximizing the EE ratio in (10) while considering different constraints on the precoder design provides us the optimal number of RF chains.

A. Problem Formulation

For a point-to-point A/D hybrid MIMO system, as shown in Fig. 1, the overall achievable rate with respect to the active RF chains can be expressed as follows:

$$R(\mathbf{P}_{\mathrm{TX}}, \mathbf{P}_{\mathrm{RX}}) = \log \left|\mathbf{I}_{N_s} + \frac{1}{\sigma_{\mathrm{n}}^{2}} \mathbf{W}_{\mathrm{BB}}^{H} \mathbf{P}_{\mathrm{RX}}^{\frac{1}{2}} \mathbf{W}_{\mathrm{RF}}^{H} \mathbf{H} \mathbf{F}_{\mathrm{RF}} \times \mathbf{P}_{\mathrm{TX}}^{\frac{1}{2}} \hat{\mathbf{F}}_{\mathrm{BB}} \hat{\mathbf{F}}_{\mathrm{BB}}^{H} \mathbf{P}_{\mathrm{TX}}^{\frac{1}{2}} \mathbf{F}_{\mathrm{RF}}^{H} \mathbf{H}^{H} \mathbf{W}_{\mathrm{RF}} \mathbf{P}_{\mathrm{RX}}^{\frac{1}{2}} \mathbf{W}_{\mathrm{BB}}\right|, \tag{11}$$

where $\mathbf{P}_{\mathrm{TX}} \in \mathbb{R}^{L_{\mathrm{T}} \times L_{\mathrm{T}}}$ is the diagonal matrix describing the power allocation for the TX. For the RX, we use the diagonal matrix $\mathbf{P}_{\mathrm{RX}} \in \{0,1\}^{L_{\mathrm{R}} \times L_{\mathrm{R}}}$ which takes only values from $\{0,1\}$, since it only represents a switching network, hence, $L_{\mathrm{R}}^{opt} = \|\mathbf{P}_{\mathrm{RX}}\|_{0}$.

Based on [15], it is reasonable to assume that $\hat{\mathbf{F}}_{\mathrm{BB}}\hat{\mathbf{F}}_{\mathrm{BB}}^{H} \approx \mathbf{I}_{L_{\mathrm{T}}}$ and $\mathbf{W}_{\mathrm{BB}}\mathbf{W}_{\mathrm{BB}}^{H} \approx \mathbf{I}_{L_{\mathrm{R}}}$, then

$$R(\mathbf{P}_{\mathrm{TX}}, \mathbf{P}_{\mathrm{RX}}) = \log|\mathbf{I}_{L_{\mathrm{R}}} + \frac{1}{\sigma_{\mathrm{n}}^2}\mathbf{P}_{\mathrm{RX}}^{\frac{1}{2}}\mathbf{W}_{\mathrm{RF}}^{H}\mathbf{H}\mathbf{F}_{\mathrm{RF}} \mathbf{P}_{\mathrm{TX}}\mathbf{F}_{\mathrm{RF}}^{H}\mathbf{H}^{H}\mathbf{W}_{\mathrm{RF}}\mathbf{P}_{\mathrm{RX}}^{\frac{1}{2}}|. \tag{12}$$

To simplify this problem, we decompose it into two successive sub-problems, one for the TX and one for the RX. Specifically, to obtain $\mathbf{P}_{\mathrm{TX}}$ we assume that the RX has activated all the switches, i.e., $\mathbf{P}_{\mathrm{RX}} = \mathbf{I}_{L_{\mathrm{R}}}$. So,

$$R(\mathbf{P}_{\mathrm{TX}}) = \log|\mathbf{I}_{L_{\mathrm{R}}} + \frac{1}{\sigma_{\mathrm{n}}^2}\mathbf{W}_{\mathrm{RF}}^{H}\mathbf{H}\mathbf{F}_{\mathrm{RF}}\mathbf{P}_{\mathrm{TX}}\mathbf{F}_{\mathrm{RF}}^{H}\mathbf{H}^{H}\mathbf{W}_{\mathrm{RF}}|. \tag{13}$$

Once we obtain $\mathbf{P}_{\mathrm{TX}}$, we can estimate $\mathbf{P}_{\mathrm{RX}}$ based on the following formulation:

$$R(\mathbf{P}_{\mathrm{RX}}) = \log\left|\mathbf{I}_{L_{\mathrm{R}}} + \frac{1}{\sigma_{\mathrm{n}}^2}\mathbf{P}_{\mathrm{RX}}^{\frac{1}{2}}\mathbf{W}_{\mathrm{RF}}^{H}\mathbf{H}\mathbf{F}_{\mathrm{RF}} \mathbf{P}_{\mathrm{TX}}\mathbf{F}_{\mathrm{RF}}^{H}\mathbf{H}^{H}\mathbf{W}_{\mathrm{RF}}\mathbf{P}_{\mathrm{RX}}^{\frac{1}{2}}\right|. \tag{14}$$

Maximizing EE at the RX using (14) results into a non-trivial integer programming problem. Therefore in the following we will focus our analysis on the EE maximization at the TX in order to obtain L_{T}^{opt}. We consider the optimal number of RF chains at the RX to be same as at the TX, i.e., $L_{\mathrm{R}}^{opt} = L_{\mathrm{T}}^{opt}$.

Measuring the energy consumed for each entity in the precoder and the combiner is important to design an energy efficient mmWave A/D hybrid MIMO system. Similarly to [9], [19], that total power *P* for an A/D hybrid beamforming system can be described as follows, where we include the power consumed by the RX components as well:

$$P = \beta\mathrm{tr}(\mathbf{P}_{\mathrm{TX}}) + 2P_{\mathrm{CP}} + N_{\mathrm{T}}P_{\mathrm{T}} + N_{\mathrm{R}}P_{\mathrm{R}} + L_{\mathrm{T}}^{opt} \times (P_{\mathrm{RF}} + N_{\mathrm{T}}P_{\mathrm{PS}}) + L_{\mathrm{R}}^{opt}(P_{\mathrm{RF}} + N_{\mathrm{R}}P_{\mathrm{PS}})(\mathrm{W}), \tag{15}$$

where β represents the reciprocal of amplifier efficiency; the common parameters at the TX and the RX are P_{CP}, P_{RF}, and P_{PS} which represent the common power, the power per RF chain, and the power per phase shifter, respectively. P_{T} and P_{R} represent the power per antenna element at the TX and the RX, respectively.

For simplicity we remove the sub-index term "TX" from $\mathbf{P}_{\mathrm{TX}}$. Hence, we consider the problem (10) expressed with respect to the power allocation matrix $\mathbf{P} \in \mathbb{R}^{L_{\mathrm{T}}\times L_{\mathrm{T}}}$ as follows:

$$\max_{\mathbf{P}\in\mathcal{D}^{L_{\mathrm{T}}\times L_{\mathrm{T}}}} \frac{R(\mathbf{P})}{P(\mathbf{P})} \,\mathrm{s.t.}\, P(\mathbf{P}) \le P'_{\max} \mathrm{and}\, R(\mathbf{P}) \ge R_{\min}. \tag{16}$$

The first constraint term in (16) sets the upper bound for the total power budget of the communication system, i.e., $P'_{\max} = \beta P_{\max} + 2P_{\mathrm{CP}} + N_{\mathrm{T}}P_{\mathrm{T}} + N_{\mathrm{R}}P_{\mathrm{R}} + L_{\mathrm{T}} \times (P_{\mathrm{RF}} + N_{\mathrm{T}}P_{\mathrm{PS}}) + L_{\mathrm{R}}(P_{\mathrm{RF}} + N_{\mathrm{R}}P_{\mathrm{PS}})$.

B. Dinkelbach Method (DM) Based Proposed Solution

Fractional programming theory provides us several options to obtain the solution of (16). One computational efficient algorithm is the Dinkelbach's algorithm which has been introduced firstly in [33], [34]. Dinkelbach's algorithm replaces the fractional cost function of (16) with a sequence of easier difference-based problems. The simulation results in Section V suggest that this method can achieve good performance. Specifically, the cost function of (16) is replaced by a sequence of problems:

$$\max_{\mathbf{P}^{(m)}\in\mathcal{D}^{L_{\mathrm{T}}\times L_{\mathrm{T}}}} \left\{R\left(\mathbf{P}^{(m)}\right) - \nu^{(m)}P\left(\mathbf{P}^{(m)}\right)\right\}, \tag{17}$$

where $\nu^{(m)} = R(\mathbf{P}^{(m-1)})/P(\mathbf{P}^{(m-1)}) \in \mathbb{R}^{+}$, for $m = 1, 2, \ldots, I_{\max}$, where $I_{\max}$ is the number of maximum iterations. Dinkelbach's algorithm is an iterative algorithm, where at each step an update of $\nu^{(m)}$ is obtained based on the estimated rate and power from the previous iteration. To simplify the implementation of this algorithm we desire a rate expression that does not require explicit formulas for the precoder and combiner matrices, thus avoiding re-running Algorithms 1 and 2 for each possible choice of active RF chains.

In order to proceed with the Dinkelbach's algorithm in our context, let us first elaborate on the information rate and power expressions. Considering the SVD of the channel as $\mathbf{H} = \mathbf{U}_{\mathrm{H}}\mathbf{\Sigma}_{\mathrm{H}}\mathbf{V}_{\mathrm{H}}^{H}$ as shown in Section III-A, (13) is expressed as:

$$R(\mathbf{P}) = \log|\mathbf{I}_{N_{\mathrm{R}}} + \frac{1}{\sigma_{\mathrm{n}}^2}\mathbf{W}_{\mathrm{RF}}^{H}\mathbf{U}_{\mathrm{H}}\mathbf{\Sigma}_{\mathrm{H}}\mathbf{V}_{\mathrm{H}}^{H}\mathbf{F}_{\mathrm{RF}} \times \mathbf{P}\mathbf{F}_{\mathrm{RF}}^{H}\mathbf{V}_{\mathrm{H}}\mathbf{\Sigma}_{\mathrm{H}}^{H}\mathbf{U}_{\mathrm{H}}^{H}\mathbf{W}_{\mathrm{RF}}|. \tag{18}$$

Following the analysis of [15], it can be proven that $\mathbf{V}_{\mathrm{H}}^{H}\mathbf{F}_{\mathrm{RF}} \approx [\mathbf{I}_{L_{\mathrm{T}}}\, \mathbf{0}_{(N_{\mathrm{T}}-L_{\mathrm{T}})\times L_{\mathrm{T}}}^{T}]^{T}$ and $\mathbf{U}_{\mathrm{H}}^{H}\mathbf{W}_{\mathrm{RF}} \approx [\mathbf{I}_{L_{\mathrm{R}}}\, \mathbf{0}_{(N_{\mathrm{R}}-L_{\mathrm{R}})\times L_{\mathrm{R}}}^{T}]^{T}$, hence,

$$R(\mathbf{P}) = \log|\mathbf{I}_{N_{\mathrm{R}}} + \frac{1}{\sigma_{\mathrm{n}}^2}\bar{\mathbf{\Sigma}}^2\mathbf{P}|, \tag{19}$$

where $\bar{\mathbf{\Sigma}} \in \mathbb{R}^{L_{\mathrm{R}}\times L_{\mathrm{T}}}$ with $[\bar{\mathbf{\Sigma}}]_{kk} = [\mathbf{\Sigma}_{\mathrm{H}}]_{kk}$ for $k = 1, \ldots, L_{\mathrm{T}}$, assuming $L_{\mathrm{T}} = L_{\mathrm{R}}$, while its remaining entries are zero. Since the involved matrices in (19) are diagonal, the information rate is decomposed into L_{T} parallel streams, as follows:

$$R(\mathbf{P}) \approx \sum_{k=1}^{L_{\mathrm{T}}} \log\left(1 + \frac{1}{\sigma_{\mathrm{n}}^2}\left[\bar{\mathbf{\Sigma}}^2\right]_{kk}[\mathbf{P}]_{kk}\right)(\mathrm{bits/s/Hz}). \tag{20}$$

Recall that L_{T} and L_{R} have preset values based on the hardware design and describe the available RF chains at the TX and the RX, respectively. Considering only the TX, the consumed power with respect to the diagonal power allocation matrix can be written as:

$$P_{\mathrm{TX}}(\mathbf{P}) = P_{\mathrm{static}} + \sum_{k=1}^{L_{\mathrm{T}}}(\beta[\mathbf{P}]_{kk} + P_{\mathrm{RF}} + N_{\mathrm{T}}P_{\mathrm{PS}}) \tag{21}$$

$$= P_{\mathrm{static}} + \sum_{k=1}^{L_{\mathrm{T}}}\beta'[\mathbf{P}]_{kk}(\mathrm{W}), \tag{22}$$

Algorithm 3 Dinkelbach Method (DM) Based Solution

1: **Initialize:** $\mathbf{P}^{(0)}, \nu^{(0)}$ satisfying $\mathcal{G}(\mathbf{P}^{(0)}, \nu^{(0)}) \geq 0$, L_{T}, tolerance ϵ
2: $m = 0$
3: **while** $|\mathcal{G}(\mathbf{P}^{(m)}, \nu^{(m)})| > \epsilon$ **do**
4: Update $\mathbf{P}^{(m)}$ by solving the relaxation of (23) via CVX [35].
5: Thresholding $\mathbf{P}^{(m)}$ as $\mathbf{P}_{\mathrm{th}}^{(m)}$.
6: Counting non-zero values of $\mathbf{P}_{\mathrm{th}}^{(m)}$ provides L_{T}^{opt}.
7: Compute $R(\mathbf{P}^{(m)})$ and $P_{\mathrm{TX}}(\mathbf{P}^{(m)})$.
8: Compute $\mathcal{G}(\mathbf{P}^{(m)}, \nu^{(m)})$ where $\nu^{(m)} = R(\mathbf{P}^{(m-1)})/P(\mathbf{P}^{(m-1)}) \in \mathbb{R}^{+}$.
9: Update $\nu^{(m)}$ with $R(\mathbf{P}^{(m)})/P_{\mathrm{TX}}(\mathbf{P}^{(m)})$.
10: $m = m{+}1$
11: **end while**
12: Obtain $L_{\mathrm{T}}^{opt} = \|\mathbf{P}_{\mathrm{th}}^{(m)}\|_0$

Algorithm 4 Full Search (FS) Approach

1: **Initialize:** L_{T}, tolerance ϵ, $\mathrm{EE}^{(0)} = 0$
2: **for** $i = 1 : L_{\mathrm{T}}$
3: **while** $|\mathcal{G}(\mathbf{P}^{(m)}, \nu^{(m)})| > \epsilon$ **do**
4: Compute $\mathbf{P}^{(m)}$ subject to i RF chains $\rightarrow$ obtain L_{T}^{opt} from $\mathbf{P}_{\mathrm{th}}^{(m)}$.
5: Compute $R(\mathbf{P}^{(m)})$, $P_{\mathrm{TX}}(\mathbf{P}^{(m)})$ and $\mathcal{G}(\mathbf{P}^{(m)}, \nu^{(m)})$.
6: Update $\nu^{(m)}$ and compute $\mathrm{EE}^{(m)} = R(\mathbf{P}^{(m)})/P_{\mathrm{TX}}(\mathbf{P}^{(m)})$.
7: $m = m{+}1$
8: **end while**
9: Obtain $L_{\mathrm{T}}^{(i)} = L_{\mathrm{T}}^{opt}$ and $\mathrm{EE}^{(i)}$ based on $\mathrm{EE}^{(m)}$ value.
10: **if** $\mathrm{EE}^{(i)} \geq$ previous $\mathrm{EE}^{(i-1)}$
11: Update $\mathrm{EE}^{(i)}$ and $L_{\mathrm{T}}^{(i)}$
12: **end if**
13: **end for**

where $P_{\mathrm{static}} \triangleq P_{\mathrm{CP}} + N_{\mathrm{T}}P_{\mathrm{T}}$ is independent of the power allocation matrix $\mathbf{P}$ and $\beta' \triangleq \beta + \frac{P_{\mathrm{RF}}+N_{\mathrm{T}}P_{\mathrm{PS}}}{P_{\max}}$. The equivalence between (21) and (22) is justified since $\sum_{k=1}^{L_{\mathrm{T}}}[\mathbf{P}]_{kk} = \mathrm{tr}(\mathbf{P}) = P_{\max}$.

Based on (20) and (22), the m-th Dinkelbach method (DM) step can be expressed as follows:

$$\left\{\mathbf{P}^{(m)}, \nu^{(m)}\right\} = \arg \max_{\mathbf{P}^{(m)} \in \mathcal{D}^{L_{\mathrm{T}} \times L_{\mathrm{T}}}} \mathcal{G}\left(\mathbf{P}^{(m)}, \nu^{(m)}\right), \quad (23)$$

where

$$\mathcal{G}\left(\mathbf{P}^{(m)}, \nu^{(m)}\right) \triangleq \sum_{k=1}^{L_{\mathrm{T}}} \log\left(1 + \frac{1}{\sigma_{\mathrm{n}}^2}\left[\bar{\mathbf{\Sigma}}^2\right]_{kk}\left[\mathbf{P}^{(m)}\right]_{kk}\right) - \nu^{(m)} \sum_{k=1}^{L_{\mathrm{T}}} \beta'\left[\mathbf{P}^{(m)}\right]_{kk}. \quad (24)$$

Note that problem (23) is a non-convex one because of the constraint $\mathbf{P}^{(m)} \in \mathcal{D}^{L_{\mathrm{T}} \times L_{\mathrm{T}}}$. To proceed, first we alleviate this constraint, thus (23) can be efficiently solved by any standard interior-point method (for example, CVX [35]). Step 3 of Algorithm 3 shows that after alleviating this constraint, (23) is solved via CVX to update $\mathbf{P}^{(m)}$. Then we impose the constraint by hard-thresholding the entries of $\mathbf{P}^{(m)}$, i.e., $\mathbf{P}_{\mathrm{th}}^{(m)}$, as shown in Step 4 of Algorithm 3. The thresholding sets to zero all entries of $\mathbf{P}^{(m)}$ that are lower than a given tolerance value ϵ_{th}.

Algorithm 3 starts by initializing the number of available RF chains L_{T}. We update $\mathbf{P}^{(m)}$ by solving the relaxation of (23) via CVX as shown in Step 3. Steps 4-5 show that $\mathbf{P}^{(m)}$ is thresholded as $\mathbf{P}_{\mathrm{th}}^{(m)}$ and counting its non-zero values provides us the optimal number of RF chains which keeps updating within the loop but obtained as $\|\mathbf{P}_{\mathrm{th}}^{(m)}\|_0$ after the loop ends as shown in Step 11. $R(\mathbf{P}^{(m)})$ and $P_{\mathrm{TX}}(\mathbf{P}^{(m)})$ are computed in Step 6 and $\mathcal{G}(\mathbf{P}^{(m)}, \nu^{(m)})$ is computed based on (24) in Step 7 where $\nu^{(m)} = R(\mathbf{P}^{(m-1)})/P(\mathbf{P}^{(m-1)}) \in \mathbb{R}^{+}$. Steps 8 shows the update in $\nu^{(m)}$ with $R(\mathbf{P}^{(m)})/P_{\mathrm{TX}}(\mathbf{P}^{(m)})$. The loop continues until $|\mathcal{G}(\mathbf{P}^{(m)}, \nu^{(m)})|$ is less than a given tolerance ϵ. We consider that the optimal number of RF chains provides the number of data streams as well, i.e., $N_{\mathrm{s}} = L_{\mathrm{T}}^{opt}$.

C. Full Search (FS) Approach

To show that the loss performance is not much in Dinkelbach optimization we also consider a full search (FS) approach which resolves the non-convexity issue of (23) with convex approximation providing a modified version of the proposed Dinklbach optimization solution which iterates over all the possible number of RF chains. The steps are stated in Algorithm 4 where the maximum energy efficiency "EE" is obtained and the corresponding number of RF chains are considered to be optimal at the end of the algorithm. In Table IV of Section V, we show that the proposed DM has similar performance to the FS approach, while the complexity for computing FS increases significantly.

D. Brute Force (BF) Approach

The solution to achieve optimal number of RF chains at each realization is also provided in [22] which we call as the brute force (BF) approach. To make the A/D hybrid beamforming system energy efficient, BF approach, at each realization (current channel condition), makes a search on all the possible number of RF chains, i.e., $L_{\mathrm{T}} = \{1, 2, 3, \ldots, N_{\mathrm{T}}\}$, and computes best energy efficiency while designing the precoder and combiner matrices, and chooses the corresponding number of RF chains as the optimal number of RF chains. We, in our work, mitigate that need of searching for all possible number of RF chains and then finding an optimal solution, and thus providing equally a high energy efficient and low complexity solution. The observations made in the next section support this statement.

V. Simulation Results

This section shows the performance of the proposed DM compared to the existing state of the art solutions such as the BF approach, digital beamforming, analog beamforming and modified version of the proposed solution, i.e., FS

approach. For simulations, the proposed DM and the FS approach consider $L_{\mathrm{T}} = L_{\mathrm{R}} = \mathrm{length}(\mathrm{eig}(\mathbf{H}\mathbf{H}^H))$ and the BF approach uses the same precoding and combining matrices as the DM solution. The tolerance values considered in both the DM solution and the FS approach algorithms are $\epsilon = 10^{-4}$ and $\epsilon_{\mathrm{th}} = 10^{-6}$. The fully digital beamforming solution uses the same number of RF chains as antennas, i.e., $L_{\mathrm{T}} = N_{\mathrm{T}}$ and $L_{\mathrm{R}} = N_{\mathrm{R}}$, and precoding and combining matrices are $\mathbf{F}_{\mathrm{opt}}$ and $\mathbf{W}_{\mathrm{mmse}}$, respectively, as shown in Sections III-A and III-B. The analog beamforming solution implements a single RF chain, i.e., $L_{\mathrm{T}} = L_{\mathrm{R}} = 1$, and the precoding and combining matrices are computed as the phases of the first singular vectors, i.e., $\mathbf{F} = \mathbf{V}_{\mathrm{H}}(1:N_{\mathrm{T}},1)/\mathrm{abs}(\mathbf{V}_{\mathrm{H}})$ and $\mathbf{W} = \mathbf{U}_{\mathrm{H}}(1:N_{\mathrm{R}},1)/\mathrm{abs}(\mathbf{U}_{\mathrm{H}})$, respectively.

The performance of the codebook-free designs such as ADMM [16] and SVD based [12] solutions when incorporated with the proposed framework, using L_{T}^{opt} RF chains, are also observed over the case when fixed number of RF chains are used to compute the precoder and combiner matrices. The comparison between GP and OMP algorithms is also observed through observing the variations in run time with respect to the number of RF chains and computational complexities.

A. System Setup

For the channel parameters, there are 10 rays for each cluster and there are 8 clusters in total, i.e., $N_{\mathrm{ray}} = 10$ and $N_{\mathrm{cl}} = 8$ in (1). The average power of each cluster is unity, i.e., $\sigma_{\alpha,i} = 1$. The azimuth and elevation angles of departure and arrival are computed on the basis of the Laplacian distribution [36] with uniformly distributed mean angles and angle spread as 7.5°. The mean angles are sectored within the range of 60° to 120° in the azimuth domain, and 80° to 100° in the elevation domain. The 64 antenna elements at the TX, i.e., $N_{\mathrm{T}} = 64$, and 16 at the RX, i.e., $N_{\mathrm{R}} = 16$, in the ULA, antenna elements are spaced by distance $d = \lambda/2$ where $\lambda/2$ can be based on a standard frequency value such as 28 GHz [22]. The system bandwidth is normalized to 1 Hz in the simulations. The signal to noise ratio (SNR) is $1/\sigma_{\mathrm{n}}^2$. All the simulation results are averaged over 1000 random channel realizations. To illustrate the achievable energy efficiency of different precoding solutions, the parameters in the power expressions for each precoder design are set as shown in Table I(a). For a typical case, the power per power amplifier, $P_{\mathrm{PA}} = 300$ mW, and maximum achievable power, $P_{\max} = 1$ W. Table I(b) shows the maximum power which can be consumed as determined in (15) for different number of RF chains in a 64 × 16 fully-connected system. The amplifier efficiency $1/\beta$ is considered as 0.4 and the minimum desired rate in (16), $R_{\min} = 1$ bits/s/Hz.

B. Beam Training and Data Communications Phases Analysis

Based on the described communication phases in Fig. 1(b), there are L_{T} active RF chains during the beam training phase.

TABLE I
SIMULATION PARAMETERS FOR THE POWER EXPRESSIONS OF DIFFERENT PRECODING SOLUTIONS

Common power of TX	P_{CP} = 10 W
Power per RF chain	P_{RF} = 100 mW
Power per phase shifter	P_{PS} = 10 mW

(a) Typical values of the power terms [37].

Number of RF chains, L_{T}	Maximum consumed power (W)
4	34.50
8	38.50
64	94.50

(b) Maximum consumed power in (15) for different values of L_{T} for a 64 × 16 system with $\mathrm{tr}(\mathbf{F}\mathbf{F}^H) = 1$.

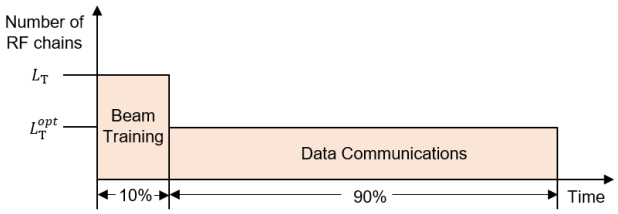

(a) Beam training and data communications phases.

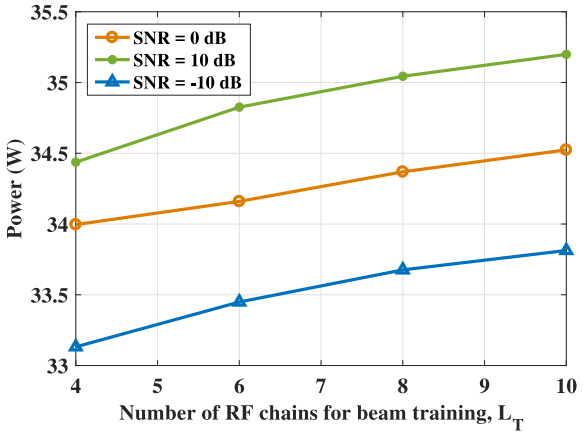

(b) Overall power consumption performance for 10% beam training and 90% data communications phases.

Fig. 2. Beam training and data communications phases and associated power consumption performance for a fully-connected 64 × 16 system.

Once the Dinkelbach or FS optimization is performed then we obtain the optimal number L_{T}^{opt} RF chains for the data communications phase. Considering that α represents the ratio between the two phases, the power consumption performance for both the stages is given by:

$$\mathrm{Power} = \alpha \times P(L_{\mathrm{T}}) + (1-\alpha) \times P\left(L_{\mathrm{T}}^{opt}\right)(\mathrm{W}), \quad (25)$$

where $P(L_{\mathrm{T}})$ is the power consumption with (15) using L_{T} RF chains and $P(L_{\mathrm{T}}^{opt})$ is using the optimal number of RF chains, L_{T}^{opt}. For example, as shown in Fig. 2(a), when

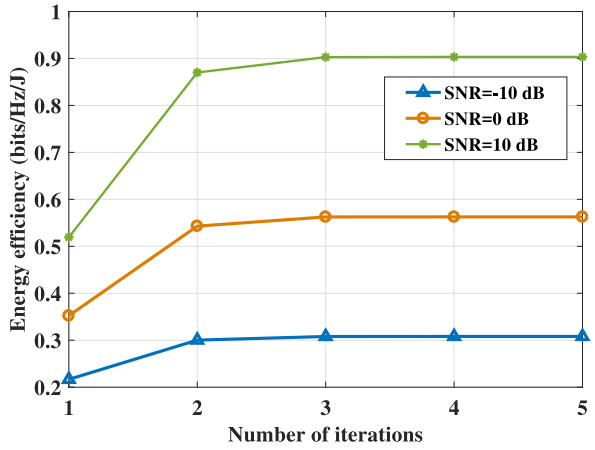

(a) Convergence of the proposed DM for different SNR levels.

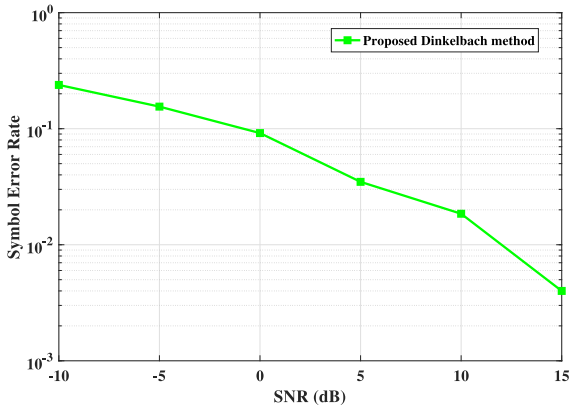

(b) Symbol error rate (SER) vs SNR for the proposed DM with Q-PSK modulation.

Fig. 3. Convergence and SER accuracy performance of the proposed DM solution for a fully-connected 64 × 16 system.

we consider that the beam training phase is active for 10% of the time with L_{T} RF chains, i.e., $\alpha = 0.1$, and the data communications phase is active for the remaining 90% time with L_{T}^{opt} RF chains, i.e., $1 - \alpha = 0.9$. The performance is observed with three SNR cases in Fig. 2(b). It can be observed that the overall power consumption increases with the increase in the number of RF chains in the beam training phase and high SNR values have higher power consumption levels. For example, at $L_{\mathrm{T}} = 6$, the power consumption at SNR $= 0$ dB is about 0.65 W higher than at SNR $= -10$ dB.

C. Convergence and Accuracy Performance of the DM

Fig. 3(a) shows the convergence of the Dinkelbach optimization solution as proposed in Algorithm 3 to obtain the optimal number of RF chains. It can be observed that the energy efficiency for different SNR levels increases with the iterations used to find the optimal number of RF chains. The proposed solution converges rapidly and needs only 2 iterations to converge and achieve an optimal solution at each realization. To express the accuracy performance of the proposed DM, Fig. 3(b) shows the symbol error rate (SER) versus SNR plot for quadrature phase shift keying (QPSK) modulation where SER decreases with the increase in SNR.

TABLE II
COMPUTATIONAL COMPLEXITY COMPARISON BETWEEN DM AND BF SOLUTIONS

Algorithm	Complexity Order
Dinkelbach	$\mathcal{O}(L_{\mathrm{T}}^{opt})$
Brute force	$\mathcal{O}(L_{\mathrm{T}}^{opt} N_{\mathrm{T}})$

(a) Complexity orders of DM and BF.

No. of TX antennas, N_{T}	Time (s): DM	Time (s): BF
80	4.29	6.13
96	4.38	10.6
112	4.54	17.6
128	4.55	26.9

(b) Run time comparison w.r.t. N_{T} at SNR = 10 dB and $P_{\max} = 1$.

D. Proposed DM Versus BF Approach

The comparison is made to the BF method [22] in detail in terms of the probability mass function (PMF) for RF chain selection, energy efficiency performance and the computational complexity. The PMF plots indicate the histogram that for how many realizations (on *y*-axis) a particular value of the variable defined on *x*-axis is achieved. Figs. 4 and 5 show the PMF of the distribution of the proposed DM and the BF approach over the optimal number of RF chains, i.e., L_{T}^{opt}, their difference, i.e., $\Delta L_{\mathrm{T}}^{opt} = |L_{\mathrm{T}\ \mathrm{BF}}^{opt} - L_{\mathrm{T}\ \mathrm{DM}}^{opt}|$, and the energy efficiency difference, i.e., $\Delta \mathrm{E} = |\mathrm{EE}_{\mathrm{BF}} - \mathrm{EE}_{\mathrm{DM}}|$, at each channel realization. Fig. 4 shows that for how many channel realizations, the beamforming solutions such as the DM and the BF approach find a particular optimal number of RF chains for different values of $P_{\max}$. It gives us an idea on how close the proposed DM solution is to the BF technique, in terms of finding the optimal number of RF chains. For example, at $P_{\max} = 1$ W, the DM solution chooses $L_{\mathrm{T}}^{opt} = 4$ for ≈ 750 different channel realizations whereas BF chooses 4 RF chains for ≈ 300 realizations and the difference (at each realization) between chosen optimal number of RF chains by both the methods, i.e., $\Delta L_{\mathrm{T}}^{opt}$ is 0 for ≈ 450 different realizations. Also, for example, the energy efficiency difference between the two methods, Δ E, at $P_{\max} = 1$ W is close to 0 bits/Hz/J for ≈ 650 channel realizations as observed from Fig. 5.

Table II(a) shows the computational complexities used by the solutions of the BF approach and the DM with respect to the number of the RF chains. We can observe that complexity for the solution of the DM requires complexity order of only $\mathcal{O}(L_{\mathrm{T}}^{opt})$ per iteration. Since the number of the required iterations is usually very small, the overall complexity of the DM is much less than the BF approach which depends on the product of the number of RF chains and the number of antennas. This is also verified by the run time results as shown in Table II(b). At SNR $= 10$ dB and $P_{\max} = 1$, the run time (in seconds) is much less for the proposed solution with respect to (w.r.t.) the number of TX antennas. These results are reported from MATLAB simulation runtime for 10 independent channel realizations. For example, for a large

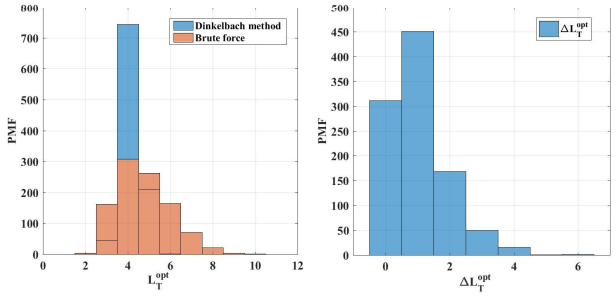

(a) $P_{\max} = 1$ W.

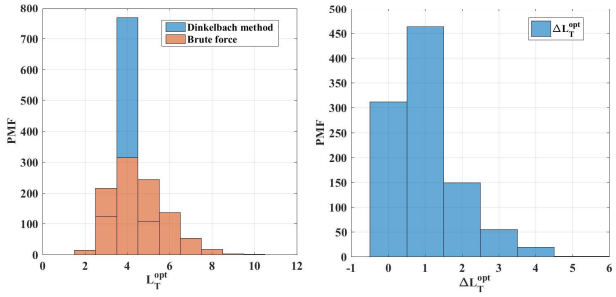

(b) $P_{\max} = 0.5$ W.

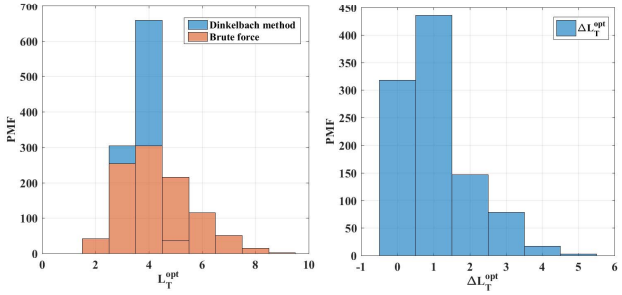

(c) $P_{\max} = 0.25$ W.

Fig. 4. PMF plots of the DM and BF solutions at different $P_{\max}$ values for the optimal number of RF chains L_{T}^{opt} and their difference $\Delta L_{\mathrm{T}}^{opt}$ for 64×16 system and SNR $= 10$ dB.

number of antennas, i.e., $N_{\mathrm{T}} = 128$, the proposed solution consumes ≈ 6 times less run time than the BF solution. The observations support the statement that the proposed solution has low complexity while still optimizing the number of RF chains.

E. Proposed GP Versus OMP

Concerning the complexity for deriving the beamforming matrices, recall that OMP requires inversion of a matrix with size $k \times k$, at each one of the L_{T}^{opt} iterations in total, with $k = 1, \ldots, L_{\mathrm{T}}^{opt}$. This operation has cubic complexity order with respect to the size of the matrix, i.e., $\mathcal{O}(k^3)$, in general. So, for L_{T}^{opt} iterations, the total cost would be:

$$\sum_{k=1}^{L_{\mathrm{T}}^{opt}} \mathcal{O}\left(k^3\right) = \mathcal{O}\left(\left(L_{\mathrm{T}}^{opt}\right)^4\right). \tag{26}$$

Additionally, a matrix-matrix product is required at each iteration with total cost $\mathcal{O}((L_{\mathrm{T}}^{opt})^3 N_{\mathrm{T}})$. On the other side,

TABLE III
COMPUTATIONAL COMPLEXITY COMPARISON BETWEEN GP AND OMP SOLUTIONS

Algorithm	Complexity Order
OMP	$\mathcal{O}\left((L_{\mathrm{T}}^{opt})^4\right) + \mathcal{O}\left((L_{\mathrm{T}}^{opt})^3 N_{\mathrm{T}}\right)$
GP	$\mathcal{O}\left((L_{\mathrm{T}}^{opt})^3 N_{\mathrm{T}}\right)$

(a) Complexity orders of GP and OMP.

No. of RF chains at the TX	Time (μs): OMP	Time (μs): GP
8	1.6	1.1
16	5.8	2.8
24	10	5.0
32	16.4	8.0

(b) Run time comparison w.r.t. the number of RF chains for 64×16 mmWave system with $N_{\mathrm{cl}} = 8$, $N_{\mathrm{ray}} = 10$, and SNR $= 10$ dB.

the proposed GP algorithm requires only matrix-matrix multiplications at each iteration, hence the complexity order is $\mathcal{O}((L_{\mathrm{T}}^{opt})^3 N_{\mathrm{T}})$. This complexity reduction is justified by the substitution of the matrix inversion with a gradient step. The derived complexity orders are summarized in Table III(a). In Table III(b) we show the MATLAB run time comparison (in μs) between OMP and GP w.r.t. the number of RF chains at the TX for a 64×16 mmWave MIMO system with SNR $= 10$ dB. As the time difference between both the algorithmic solutions is considerable with the increase in the number of RF chains, the obtained values indicate that GP consumes much less time than OMP leading to a lower complexity system.

F. Performance Evaluation

Fig. 6 shows the energy efficiency and spectral efficiency performance of the proposed solution, the BF solution, the full digital solution and the analog beamforming solution w.r.t. SNR for a 64×16 mmWave MIMO system. It can be clearly observed from Fig. 6(a) that the proposed solution is as energy efficient as the BF solution, and better than the fully digital and analog beamforming solutions. For example, at 10 dB, the proposed solution has merely a energy efficiency difference of ≈ 0.01 bits/Hz/J with the BF, but shows ≈ 0.35 bits/Hz/J and ≈ 0.25 bits/Hz/J better energy efficiency than the fully digital and analog beamforming solutions, respectively. Also, for example, in Fig. 6(b) the proposed design at 10 dB shows a ≈ 10 bits/s/Hz less spectral efficiency than the fully digital solution, ≈ 10 bits/s/Hz better than analog beamforming and approximately the same performance as the BF method.

Fig. 7(a) shows the energy efficiency comparison among the solutions with partially-connected structures where each RF chain is connected to $N_{\mathrm{T}}/L_{\mathrm{T}}^{opt}$ antennas through phase shifters. We can observe similar energy efficiency performance characteristics as in Fig. 6(a); for example, the proposed solution has approximately the same energy efficiency performance as the BF method, ≈ 0.4 bits/Hz/J and ≈ 0.32 bits/Hz/J better than the fully digital and analog beamforming solutions, respectively, at SNR $= 15$ dB. Fig. 7(b) shows the energy efficiency performance comparison w.r.t. the number of TX antennas, N_{T}, for a fully-connected structure. We

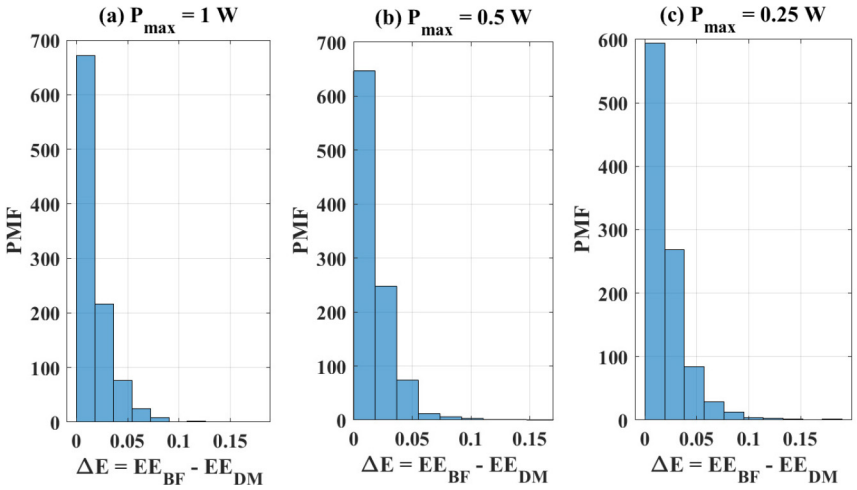

Fig. 5. PMF plots of energy efficiency difference between DM and BF solutions at different $P_{\max}$ values for a 64 × 16 system and SNR = 10 dB.

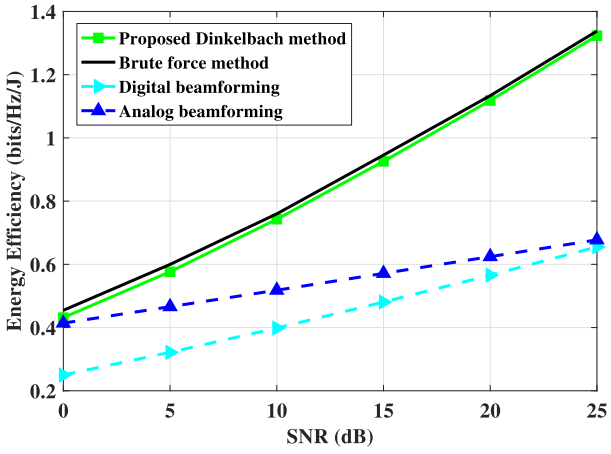

(a) Energy Efficiency w.r.t. SNR.

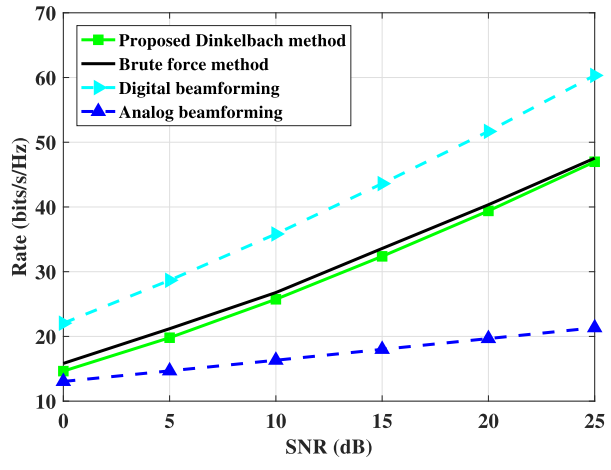

(b) Rate w.r.t. SNR.

Fig. 6. Energy efficiency and rate performance of different solutions w.r.t. SNR for a fully-connected 64 × 16 system at $P_{\max} = 1$ W.

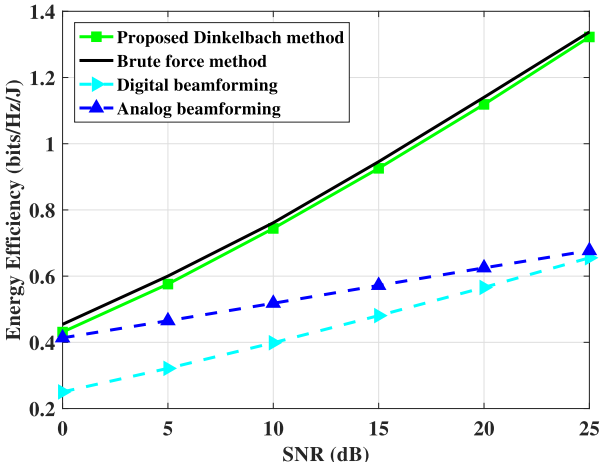

(a) w.r.t. SNR for a partially-connected structure.

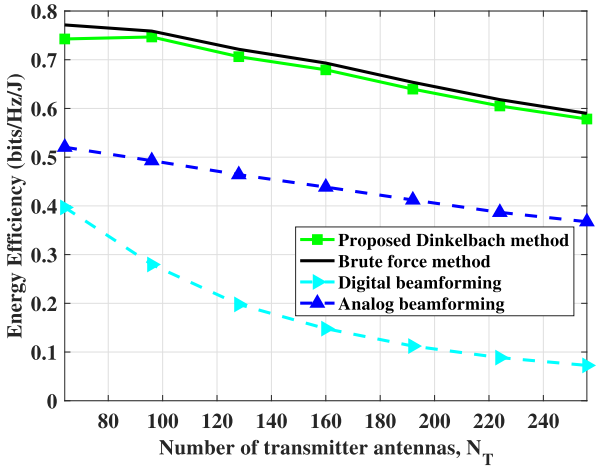

(b) w.r.t. N_{T} for a fully-connected structure.

Fig. 7. Energy efficiency performance of different solutions for a 64 × 16 hybrid mmWave MIMO system at $P_{\max} = 1$ W.

can observe that the performance starts decreasing with the increase in the number of antenna elements. For example, at $N_{\mathrm{T}} = 64$, the energy efficiency for the proposed DM is close to that of the BF solution which is ≈ 0.35 bits/Hz/J and ≈ 0.25 bits/Hz/J better than the fully digital beamforming and analog beamforming solutions, respectively. At $N_{\mathrm{T}} = 256$, the

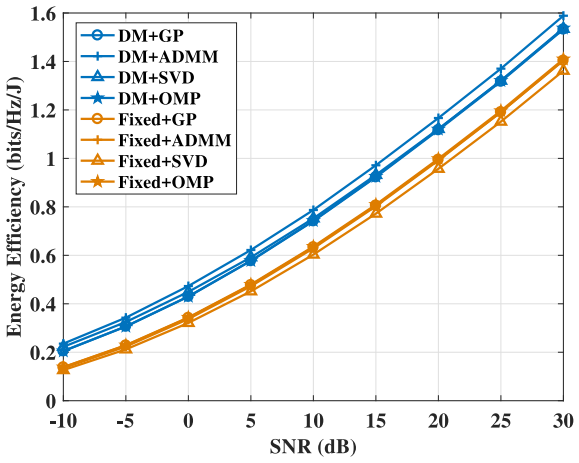

Fig. 8. Energy efficiency performance gains w.r.t. SNR at $N_{\mathrm{T}} = 64$ over the fixed number of RF chains case.

TABLE IV
ENERGY EFFICIENCY AND COMPUTATIONAL COMPLEXITY COMPARISONS BETWEEN THE PROPOSED DM AND THE FS APPROACH

SNR (dB)	$\lvert \mathrm{EE}_{\mathrm{DM}} - \mathrm{EE}_{\mathrm{FS}} \rvert$ (bits/Hz/J)
-10	0.013
-5	0.018
0	0.043
5	0.108
10	0.189

(a) Energy efficiency performance difference between the DM and the FS approach.

Algorithm	Complexity Order
Dinkelbach	$\mathcal{O}\left(L_{\mathrm{T}}^{opt}\right)$
Full search	$\mathcal{O}\left(L_{\mathrm{T}}^{opt} L_{\mathrm{T}}\right)$

(b) Complexity orders of the DM and the FS approach.

energy efficiency performance for the proposed DM solution is decreased to $\approx$ 0.56 bits/Hz/J and close to the BF solution, and $\approx$ 0.5 bits/Hz/J and $\approx$ 0.2 bits/Hz/J better than the fully digital beamforming and analog beamforming solutions, respectively.

Fig. 8 shows the energy efficiency gain of the DM based framework when used with codebook-based GP and OMP techniques, and when incorporated with codebook-free ADMM [16] and SVD [12] techniques, over the case of a fixed number of RF chains, in this case, 8. The codebook-free technique such as ADMM performs better than the codebook-based techniques such as GP and OMP, while SVD shows a similar performance. The energy efficiency performance of GP and OMP techniques are same. Table IV(a) shows energy efficiency performance comparison between the proposed DM approach (Algorithm 3), i.e., $\mathrm{EE}_{\mathrm{DM}}$, and the FS approach (Algorithm 4), i.e., $\mathrm{EE}_{\mathrm{FS}}$, where we can observe that the difference between their energy efficiency is considerably low. It states that FS approach shows very similar performance to the proposed method. From implementation perspective, Table IV(b) clearly suggests that the complexity for FS approach increases significantly as the search is made for all possible number of RF chains L_{T}.

VI. CONCLUSION

This paper proposes an energy efficient A/D hybrid beamforming framework with a novel architecture for a mmWave MIMO system, where we optimize the active number of RF chains through fractional programming. The proposed DM based framework reduces the complexity significantly and achieves almost the same energy efficiency performance as the state of the art BF approach. Both approaches achieve higher energy efficiency performance when compared with the fully digital beamforming and the analog beamforming solutions. In particular, the proposed solution only needs to compute the precoder and combiner matrices once, after the number of active RF chains are decided through the Dinkelbach optimization solution. The modified version of the proposed solution, i.e., FS approach, shows very similar performance to the proposed DM but the complexity increases significantly. The codebook-free designs such as ADMM and SVD based solutions, when incorporated with the proposed framework also achieve better energy efficiency performance over the fixed number of RF chains case. It is also shown that GP incorporated with the proposed DM is a faster and less complex approximation solution to compute the precoder and combiner matrices than OMP. For this paper, we focus on maximizing the energy efficiency but extending these techniques to consider both estimated channels and frequency selective channels can be considered for future work.

ACKNOWLEDGMENT

The authors gratefully acknowledge the Editor for coordinating the review, the anonymous reviewers for helping in revising this paper and Dr. Pan Cao for helpful discussions concerning this work.

REFERENCES

[1] Cisco Visual Mobile, *Cisco Visual Networking Index: Global Mobile Data Traffic Forecast Update, 2011–2016*, vol. 1, Cisco, San Jose, CA, USA, 2016.
[2] Z. Pi and F. Khan, "An introduction to millimeter-wave mobile broadband systems," *IEEE Commun. Mag.*, vol. 49, no. 6, pp. 101–107, Jun. 2011.
[3] S. Rangan, T. S. Rappaport, and E. Erkip, "Millimeter-wave cellular wireless networks: Potentials and challenges," *Proc. IEEE*, vol. 102, no. 3, pp. 366–385, Mar. 2014.
[4] J. G. Andrews *et al.*, "What will 5G be?" *IEEE J. Sel. Areas Commun.*, vol. 32, no. 6, pp. 1065–1082, Jun. 2014.
[5] T. S. Rappaport *et al.*, "Millimeter wave mobile communications for 5G cellular: It will work!" *IEEE Access*, vol. 1, pp. 335–349, 2013.
[6] F. Boccardi, R. W. Heath, A. Lozano, T. L. Marzetta, and P. Popovski, "Five disruptive technology directions for 5G," *IEEE Commun. Mag.*, vol. 52, no. 2, pp. 74–80, Feb. 2014.
[7] T. S. Rappaport, G. R. MacCartney, M. K. Samimi, and S. Sun, "Wideband millimeter-wave propagation measurements and channel models for future wireless communication system design," *IEEE Trans. Commun.*, vol. 63, no. 9, pp. 3029–3056, Sep. 2015.
[8] R. W. Heath, N. González-Prelcic, S. Rangan, W. Roh, and A. M. Sayeed, "An overview of signal processing techniques for millimeter wave MIMO systems," *IEEE J. Sel. Topics Signal Process.*, vol. 10, no. 3, pp. 436–453, Apr. 2016.

[9] S. Han, C.-L. I, Z. Xu, and C. Rowell, "Large-scale antenna systems with hybrid analog and digital beamforming for millimeter wave 5G," *IEEE Commun. Mag.*, vol. 53, no. 1, pp. 186–194, Jan. 2015.
[10] O. E. Ayach, R. W. Heath, S. Abu-Surra, S. Rajagopal, and Z. Pi, "The capacity optimality of beam steering in large millimeter wave MIMO systems," in *Proc. IEEE 13th Int. Workshop Signal Process. Adv. Wireless Commun. (SPAWC)*, Jun. 2012, pp. 100–104.
[11] D. J. Love and R. W. Heath, "Equal gain transmission in multiple-input multiple-output wireless systems," *IEEE Trans. Commun.*, vol. 51, no. 7, pp. 1102–1110, Jul. 2003.
[12] X. Zhang, A. F. Molisch, and S.-Y. Kung, "Variable-phase-shift-based RF-baseband codesign for MIMO antenna selection," *IEEE Trans. Signal Process.*, vol. 53, no. 11, pp. 4091–4103, Nov. 2005.
[13] J. Ahmadi-Shokouh, S. H. Jamali, and S. Safavi-Naeini, "Optimal receive soft antenna selection for MIMO interference channels," *IEEE Trans. Wireless Commun.*, vol. 8, no. 12, pp. 5893–5903, Dec. 2009.
[14] A. Kaushik, J. Thompson, and M. Yaghoobi, "Sparse hybrid precoding and combining in millimeter wave MIMO systems," in *Proc. IET Radio Propag. Technol. 5G*, Durham, U.K., Oct. 2016, pp. 1–7.
[15] O. E. Ayach, S. Rajagopal, S. Abu-Surra, Z. Pi, and R. W. Heath, "Spatially sparse precoding in millimeter wave MIMO systems," *IEEE Trans. Wireless Commun.*, vol. 13, no. 3, pp. 1499–1513, Mar. 2014.
[16] C. G. Tsinos, S. Maleki, S. Chatzinotas, and B. Ottersten, "On the energy-efficiency of hybrid analog–digital transceivers for single- and multi-carrier large antenna array systems," in *IEEE J. Sel. Areas Commun.*, vol. 35, no. 9, pp. 1980–1995, Sep. 2017.
[17] A. Kaushik, E. Vlachos, and J. Thompson, "Energy Efficiency maximization of millimeter wave hybrid MIMO systems with low resolution DACs," in *Proc. IEEE Int. Conf. Commun. (ICC)*, Shanghai, China, May 2019, pp. 1–6.
[18] E. Vlachos, A. Kaushik, and J. Thompson, "Energy efficient transmitter with low resolution DACs for massive MIMO with partially connected hybrid architecture," in *Proc. Veh. Technol. Conf. (VTC Spring)*, Porto, Portugal, Jun. 2018, pp. 1–5,
[19] X. Yu, J.-C. Shen, J. Zhang, and K. B. Letaief, "Alternating minimization algorithms for hybrid precoding in millimeter wave MIMO systems," *IEEE J. Sel. Topics Signal Process.*, vol. 10, no. 3, pp. 485–500, Apr. 2016.
[20] X. Gao, L. Dai, S. Han, C.-L. I, and R. W. Heath, "Energy-efficient hybrid analog and digital precoding for mmWave MIMO systems with large antenna arrays," *IEEE J. Sel. Areas Commun.*, vol. 34, no. 4, pp. 998–1009, Apr. 2016.
[21] E. Björnson, L. Sanguinetti, J. Hoydis, and M. Debbah, "Optimal design of energy-efficient multi-user MIMO systems: Is massive MIMO the answer?" *IEEE Trans. Wireless Commun.*, vol. 14, no. 6, pp. 3059–3075, Jun. 2015.
[22] R. Zi, X. Ge, J. Thompson, C.-X. Wang, H. Wang, and T. Han, "Energy efficiency optimization of 5G radio frequency chain systems," *IEEE J. Sel. Areas Commun.*, vol. 34, no. 4, pp. 758–771, Apr. 2016.
[23] T. Blumensath and M. E. Davies, "Gradient pursuits," *IEEE Trans. Signal Process.*, vol. 56, no. 6, pp. 2370–2382, Jun. 2008.
[24] F. Sohrabi and W. Yu, "Hybrid digital and analog beamforming design for large-scale antenna arrays," *IEEE J. Sel. Topics Signal Process.*, vol. 10, no. 3, pp. 501–513, Apr. 2016.
[25] L. Liang, W. Xu, and X. Dong, "Low-complexity hybrid precoding in massive multiuser MIMO systems," *IEEE Wireless Commun. Lett.*, vol. 3, no. 6, pp. 653–656, Dec. 2014.
[26] S. Singh, R. Mudumbai, and U. Madhow, "Interference analysis for highly directional 60-GHz mesh networks: The case for rethinking medium access control," *IEEE/ACM Trans. Netw.*, vol. 19, no. 5, pp. 1513–1527, Oct. 2011.
[27] C. Balanis, *Antenna Theory*, 2nd ed. New York, NY, USA: Wiley, 1997.
[28] A. Kaushik, E. Vlachos, J. Thompson, and A. Perelli, "Efficient channel estimation in millimeter wave hybrid MIMO systems with low resolution ADCs," in *Proc. IEEE EUSIPCO*, Rome, Italy, Sep. 2018, pp. 1825–1829.
[29] J. Brady, N. Behdad, and A. M. Sayeed, "Beamspace MIMO for millimeter-wave communications: System architecture, modeling, analysis, and measurements," *IEEE Trans. Antennas Propag.*, vol. 61, no. 7, pp. 3814–3827, Jul. 2013.
[30] L. Dai, X. Gao, S. Han, C.-L. I, and X. Wang, "Beamspace channel estimation for millimeter-wave massive MIMO systems with lens antenna array," in *Proc. IEEE/CIC Int. Conf. Commun. China (ICCC)*, Chengdu, China, Jul. 2016, pp. 1–6.
[31] J. A. Tropp, A. C. Gilbert, and M. J. Strauss, "Algorithms for simultaneous sparse approximation. Part I: Greedy pursuit," *Signal Process.*, vol. 86, no. 3, pp. 572–588, Mar. 2006.
[32] J. A. Tropp and A. C. Gilbert, "Signal recovery from random measurements via orthogonal matching pursuit," *IEEE Trans. Inf. Theory*, vol. 53, no. 12, pp. 4655–4666, Dec. 2007.
[33] W. Dinkelbach, "On nonlinear fractional programming," *Manag. Sci.*, vol. 13, no. 7, pp. 492–498, Mar. 1967.
[34] R. Jagannathan, "On some properties of programming problems in parametric form pertaining to fractional programming," *Manag. Sci.*, vol. 12, no. 7, pp. 609–615, 1966.
[35] M. C. Grant and S. P. Boyd, "Graph implementations for nonsmooth convex programs," in *Recent Advances in Learning and Control* (Lecture Notes in Control and Information Sciences), vol. 371. London, U.K.: Springer, 2008, pp. 95–110.
[36] H. Xu, V. Kukshya, and T. S. Rappaport, "Spatial and temporal characteristics of 60-GHz indoor channels," *IEEE J. Sel. Areas Commun.*, vol. 20, no. 3, pp. 620–630, Apr. 2002.
[37] T. S. Rappaport *et al.*, *Millimeter Wave Wireless Communications*. Upper Saddle River, NJ, USA: Prentice-Hall, Sep. 2014.

Aryan Kaushik received the M.Sc. degree in telecommunications from the Hong Kong University of Science and Technology, Hong Kong, in 2015. He is currently pursuing the Ph.D. degree in communications engineering with the Institute for Digital Communications, University of Edinburgh, U.K., where he is also pursuing the postgraduate certification in academic practice with the Institute for Academic Development. He has been a Visiting Researcher with Imperial College London, U.K., in 2019; the University of Luxembourg, Luxembourg, in 2018; and Beihang University, China, in 2017 and 2018. His research interests are in the area of signal processing for communications, green wireless communications for 5G and beyond, and millimeter wave multi antenna systems.

John Thompson (F'16) is currently a Professor of signal processing and communications with the Institute for Digital Communications, University of Edinburgh, U.K. He was listed as a Highly Cited Scientist by Thomson Reuters from 2015 to 2018. He specializes in millimeter wave wireless communications, signal processing for wireless networks, smart grid concepts for energy efficiency green communications systems and networks, and rapid prototyping of MIMO detection algorithms. He has published over 300 journal and conference papers in the above areas. He has coauthored the second edition of the book entitled *Digital Signal Processing: Concepts and Applications*. He coordinated EU Marie Curie International Training Network ADVANTAGE on smart grid from 2014 to 2017. He is an Editor of the IEEE TRANSACTIONS ON GREEN COMMUNICATIONS AND NETWORKING, and Communications Magazine Green Series, a Former Founding Editor-in-Chief of *IET Signal Processing*, the Technical Programme Co-Chair of IEEE Communication Society ICC 2007 Conference and Globecom 2010 Conference, the Technical Programme Co-Chair of IEEE Vehicular Technology Society VTC Spring Conference, the Track Co-Chair of the Selected Areas in Communications Topic on Green Communication Systems and Networks at ICC 2014 Conference, a Member-at-Large of IEEE Communications Society Board of Governors from 2012 to 2014, the Tutorial Co-Chair of IEEE ICC 2015 Conference, the Technical programme Co-Chair of IEEE Smartgridcomm 2018 Conference, and the Tutorial Co-Chair of ICC 2015 Conference. He is the Local Student Counselor of the IET and the Local Liaison Officer of the U.K. Communications Chapter of the IEEE.

Evangelos Vlachos (M'19) is currently a Research Associate of signal processing for communications with the Institute for Digital Communications, University of Edinburgh, U.K. His current research focus is on the next-generation 5G wireless networks, developing efficient low-power, and low-complexity techniques, suitable for the future millimeter wave massive MIMO systems. From 2015 to 2016, he was a Post-Doctoral Researcher of computer engineering and informatics with the Laboratory of Signal Processing and Telecommunications, University of Patras, Greece, working on distributed learning for signal processing over networks, where he was a Post-Doctoral Researcher of signal processing with the Visualization and Virtual Reality Group in 2016. He participated in six research projects funded by EU. He was a recipient of the Best Paper Award from IEEE ICME in 2017.

Christos Tsinos (M'14) is currently a Research Associate with the Interdisciplinary Centre for Security, Reliability and Trust, University of Luxembourg, Luxembourg. His current research interests include signal processing for mmWave, massive MIMO, cognitive radio and satellite communications, and hyperspectral image processing. From 2014 to 2015, he was a Post-Doctoral Researcher with the University of Patras, Greece. He is currently the Principal Investigator of the project "Energy and Complexity Efficient Millimeter-Wave Large-Array Communications" funded under FNR CORE Framework and a member of the Technical Chamber of Greece.

Symeon Chatzinotas (SM'13) is currently a Senior Research Scientist and the Deputy Head of the Research Group SIGCOM with the Interdisciplinary Centre for Security, Reliability and Trust, University of Luxembourg, Luxembourg. He has worked in numerous research and development projects for the Institute of Informatics and Telecommunications, the National Center for Scientific Research "Demokritos," the Institute of Telematics and Informatics, the Center of Research and Technology Hellas, and Mobile Communications Research Group, Center of Communication Systems Research, University of Surrey, U.K. He is a Visiting Professor with the University of Parma, Italy. He has authored over 300 technical papers in refereed international journals, conferences, and scientific books. His research interests are on multiuser information theory, cooperative/cognitive communications, cross-layer wireless network optimization, and content delivery networks. He was a co-recipient of the 2014 IEEE Distinguished Contributions to Satellite Communications Award, the CROWNCOM 2015 Best Paper Award, and the 2018 EURASIP JWCN Best Paper Award.